Inorganic Chemistry

Forum Article

pubs.acs.org/IC

Proton-Coupled Electron Transfer in Molecular Electrocatalysis: Theoretical Methods and Design Principles

Brian H. Solis and Sharon Hammes-Schiffer*

Department of Chemistry, University of Illinois at Urbana−Champaign, 600 South Mathews Avenue, Urbana, Illinois 61801, United States

ABSTRACT: Molecular electrocatalysts play an essential role in a wide range of energy conversion processes. The objective of electrocatalyst design is to maximize the turnover frequency and minimize the overpotential for the overall catalytic cycle. Typically, the catalytic cycle is dominated by key proton-coupled electron transfer (PCET) processes comprised of sequential or concerted electron and proton transfer steps. Theoretical methods have been developed to investigate the mechanisms, thermodynamics, and kinetics of PCET processes in electrocatalytic cycles. Electronic structure methods can be used to calculate the reduction potentials and pK_a's and to generate thermodynamic schemes, free energy reaction pathways, and Pourbaix diagrams, which indicate the most stable species under certain conditions. These types of calculations have assisted in identifying the thermodynamically favorable mechanisms under specified experimental conditions, such as acid strength and overpotential. Such calculations have also revealed linear correlations among the thermodynamic properties, which can be used to predict the impact of modifying the ligands, substituents, or metal centers. The thermodynamic properties can be tuned with electron-withdrawing or electron-donating substituents. Ligand modification can exploit the role of noninnocent ligands. For example, ligand protonation typically decreases the overpotential. Calculations of rate constants for electron and proton transfer, as well as concerted PCET, have assisted in identifying the kinetically favorable mechanisms under specified conditions. The concerted PCET mechanism is thought to lower the overpotential required for catalysis by avoiding high-energy intermediates. Rate constant calculations have revealed that the concerted mechanism involving intramolecular proton transfer will be favored by designing more flexible ligands that facilitate the proton donor−acceptor motion while also maintaining a sufficiently short equilibrium proton donor−acceptor distance. Overall, theoretical methods have assisted in the interpretation of experimental data and the design of more effective molecular electrocatalysts.

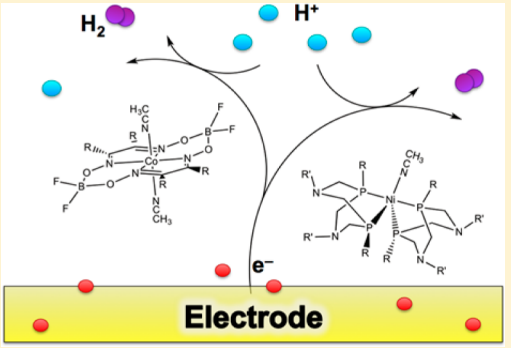

I. INTRODUCTION

Molecular electrocatalysts play an important role in a wide range of energy conversion processes, including the oxidation and production of H_2, the reduction of O_2, N_2, and CO_2, as well as the splitting of water into protons, electrons, and O_2. In efforts to design more effective electrocatalysts, the objective is to maximize the turnover frequency and minimize the overpotential for the overall catalytic cycle. Typically, the catalytic cycle is comprised of many different steps that include a number of charge transfer reactions, namely, electron transfer (ET) and proton transfer (PT). Moreover, the ET and PT steps can occur either sequentially, with ET or PT occurring first, or concertedly. Thus, many different mechanisms are possible, and the dominant mechanism is determined by a combination of thermodynamic and kinetic factors. These factors have been investigated for a variety of molecular electrocatalysts with experimental methods such as electrochemistry and nuclear magnetic resonance.[1,2] In addition, a wide range of theoretical methods have been developed to assist in the interpretation of experimental data and to guide the design of more effective molecular electrocatalysts.

This paper focuses mainly on proton-coupled electron transfer (PCET) processes in the catalytic cycles of molecular electrocatalysts. Here PCET is defined as any process that involves coupled ET and PT steps, including both sequential and concerted mechanisms.[3−8] A sequential mechanism can be confirmed by the observation of a stable intermediate. Qualitatively, a concerted mechanism is defined to be the simultaneous transfer of an electron and a proton without a stable intermediate. The rigorous definition of a stable intermediate is not straightforward, however, because of the quantum mechanical nature of the electrons and protons.[8] Moreover, the experimental observation of an intermediate relies on the experimentally accessible time scale. Nevertheless, we still utilize the qualitative definition of the concerted mechanism with these limitations in mind. We denote sequential mechanisms as ET−PT or PT−ET, corresponding to the initial transfer of the electron or proton, respectively, and concerted mechanisms as EPT. In cases where multiple electrons and protons transfer, the mechanism can be denoted

Special Issue: Insights into Spectroscopy and Reactivity from Electronic Structure Theory

Received: February 5, 2014
Published: April 14, 2014

   dx.doi.org/10.1021/ic5002896 | *Inorg. Chem.* 2014, 53, 6427−6443

as PT−PT−ET−ET, PT−EPT−ET, and so forth. Chemical intuition might suggest that the ET and PT reactions would alternate to avoid buildup of charge, resulting in steps comprised of a net hydrogen atom transfer.[9] In general, however, this type of alternation is not required and may not even be preferable from an energetic perspective. For example, a mechanism consisting of double protonation followed by reduction tends to require a lower overpotential because it is easier to reduce a species containing more positive charge. Thus, we must consider all different mechanisms and avoid focusing only on those that involve net hydrogen atom transfer steps.

The mechanism, overpotential, and turnover frequency for a given type of electrocatalyst depend on the metal center, as well as the ligands and their substituents. These properties also depend on the experimental conditions, such as the acid strength and concentration as well as the applied potential. A variety of computational methods have been developed to investigate the mechanisms of molecular electrocatalysts and to guide the design of catalysts with lower overpotentials and higher turnover frequencies. Electronic structure methods can be used to investigate the thermodynamic aspects of the catalytic cycle, namely, the relative free energies of the intermediates along various proposed reaction pathways.[10−20] A complete picture requires consideration of the kinetics as well, specifically the free energy barriers separating the intermediates. The PT rate constants can be calculated with transition state theory or more sophisticated theories that include tunneling.[21,22] The ET rate constants can be determined with Marcus theory, requiring the calculation of reorganization energies.[23] The EPT rate constants can be calculated with theories that include the quantum effects of the electrons and transferring proton, as well as the motions of the solute and solvent.[6,7,24,25] Microkinetic modeling can be used to combine all of this thermodynamic and kinetic information into a single set of coupled equations.[26−28]

An outline of this paper is as follows. Section II describes the electronic structure methods used to calculate thermodynamic properties, such as reduction potentials and pK_a's. Section III explains how this information can be used to generate thermodynamic schemes, reaction pathways, Pourbaix diagrams, and linear free energy correlations for a series of ligands and substituents. Section IV describes the role of noninnocent ligands in terms of ligand protonation and reduction, providing an example of cobalt dithiolenes for ligand protonation. Section V presents illustrative results for cobaloximes, highlighting the thermodynamic reaction pathways and linear free energy correlations. Section VI discusses the calculation of rate constants for PT, ET, and EPT reactions, with a brief discussion of microkinetic modeling. Section VII presents an illustrative example of nickel-based catalysts with pendant amines for H_2 oxidation and production, highlighting the thermodynamic schemes, Pourbaix diagrams, and rate constant calculations. An overview of catalyst design is contained in section VIII.

The goal of this Forum Article is not to provide a comprehensive review of the field but rather to provide a perspective of the role that theory and computation can play in catalyst design and to point out the limitations and challenges in this field. Although the examples provided in this paper are from our group, many other groups have contributed to this increasingly growing field. Related calculations and analyses have been performed for other molecular electrocatalysts, and similar concepts have been discussed in other contexts. Unfortunately, because of space limitations, we are unable to discuss all of this related work, and we attempt to cite it where appropriate, but we may have inadvertently missed some key references.

II. CALCULATING THERMODYNAMIC PROPERTIES

A. Reduction Potentials and pK_a's. Electronic structure methods can be used to determine thermodynamic quantities with a reasonably high level of accuracy. The standard reduction potential, E°, is determined from the calculated free energy of reduction, $\Delta G^{\circ,\mathrm{red}}_{\mathrm{solv}}$, using the relation

$$E^\circ = -\frac{\Delta G^{\circ,\mathrm{red}}_{\mathrm{solv}}}{nF} \tag{1}$$

where F is the Faraday constant and n is the number of electrons being transferred.[11] The free energy of reduction is defined as the free energy change associated with the following reaction:

$$\mathrm{Ox_{solv}} + \mathrm{e^-} \rightarrow \mathrm{Red_{solv}} \tag{2}$$

where $\mathrm{Ox_{solv}}$ and $\mathrm{Red_{solv}}$ are the oxidized and reduced species in solution.

To calculate experimentally relevant electrochemical quantities, a reference electrode must be considered. Several strategies have been employed to incorporate a reference electrode in calculations of reduction potentials. One option is to subtract a previously published experimental or theoretical value for the absolute reduction potential of the reference electrode.[10,12−14,19,20] A second option is to calculate the absolute reduction potential of the reference electrode at the same level of theory and subtract that value.[11,18,29,30] A third option is to calculate the reduction potential for a related half-cell reaction that has been experimentally studied with respect to the same reference electrode and use a thermodynamic cycle such that the reference electrodes cancel.[15−17] An advantage of the third strategy is that it avoids considering the reference electrode directly and therefore avoids any errors associated with the calculation or measurement of the reference electrode reduction potential. This strategy will be discussed in more detail in the next subsection.

The calculation of $\Delta G^{\circ,\mathrm{red}}_{\mathrm{solv}}$ with quantum chemistry methods can be performed with structures optimized in the gas phase through a Born−Haber thermodynamic cycle, shown in Scheme 1, or with structures optimized in solution. In the

Scheme 1. Born−Haber Thermodynamic Cycle for Calculating the Free Energy of Reduction

$$\begin{array}{ccc} \mathrm{Ox_{gas}} + \mathrm{e^-} & \xrightarrow{\Delta G^{\circ,\mathrm{red}}_{\mathrm{gas}}} & \mathrm{Red_{gas}} \\ \Delta G^\circ_s(\mathrm{Ox}) \downarrow \quad \downarrow & & \downarrow \Delta G^\circ_s(\mathrm{Red}) \\ \mathrm{Ox_{solv}} + \mathrm{e^-} & \xrightarrow{\Delta G^{\circ,\mathrm{red}}_{\mathrm{solv}}} & \mathrm{Red_{solv}} \end{array}$$

Born−Haber cycle, $\Delta G^{\circ,\mathrm{red}}_{\mathrm{solv}}$ is expressed in terms of the free energy of reduction in the gas phase, $\Delta G^{\circ,\mathrm{red}}_{\mathrm{gas}}$, and the solvation free energies of the reduced and oxidized species, $\Delta G^\circ_s(\mathrm{Red})$ and $\Delta G^\circ_s(\mathrm{Ox})$, respectively:

$$\Delta G^{\circ,\mathrm{red}}_{\mathrm{solv}} = \Delta G^{\circ,\mathrm{red}}_{\mathrm{gas}} + \Delta G^\circ_s(\mathrm{Red}) - \Delta G^\circ_s(\mathrm{Ox}) \tag{3}$$

The gas phase reaction free energy is calculated with the Gibbs relation

dx.doi.org/10.1021/ic5002896 | Inorg. Chem. 2014, 53, 6427−6443

$$\Delta G^{\circ}_{gas} = \Delta H^{\circ}_{gas} - T\Delta S^{\circ}_{gas} \quad (4)$$

where the change in entropy and enthalpy, including zero-point energy contributions, can be calculated with standard quantum chemistry methods. In particular, the zero-point energy contributions and the entropic effects due to the molecular vibrations are calculated from the vibrational frequencies of the normal modes using the harmonic oscillator model, and the entropic effects due to the translations and rotations are calculated using other simple models.

An alternative to using the Born−Haber cycle is to optimize the structures in solution and calculate $\Delta G^{\circ,red}_{solv}$ directly using the analogue of eq 4 with the contributions obtained from electronic structure calculations in solution.[31] When the structures optimized in the gas phase and in solution are similar, geometry optimization in the gas phase is preferable because it is computationally faster. In some cases, however, geometry optimization in solution is necessary. For example, when the gas phase structures exhibit large conformational changes due to solvation, the structures in solution are expected to be more relevant to the experimentally studied systems. Moreover, geometry optimization in solution is necessary when solvation stabilizes a particular spin state or ligand conformation that would not be found in the gas phase.[32] We emphasize that the solvent plays an important role in PCET processes, and solvent effects must be included in the calculations to obtain meaningful results. In the Born−Haber treatment, the geometry optimizations are performed in the gas phase, and the solvation free energies are calculated subsequently for these geometries. When the geometry optimizations are performed in solution, the solvation free energies are calculated during the optimizations. Thus, the significant impact of solvation on the free energies is included in both approaches.

In principle, the electron in eq 2 also contributes to the free energy associated with this reaction. When the reduction potential of the reference electrode is calculated with the same level of theory or when a separate reference half-cell reaction is considered, the effects of the electron will cancel exactly. When the absolute reduction potential of the electrode is obtained from the literature, this cancellation does not occur, and the contribution of the electron to $\Delta G^{\circ,red}_{solv}$ can be calculated with Fermi−Dirac statistics[33] in the gas phase, neglecting the solvation free energy.[11,12,34,35] The effect of the electron on the free energy is −0.868 kcal/mol at 298.15 K, which corresponds to 37.6 mV.

The pK_a is determined from the free energy of deprotonation, $\Delta G^{\circ,pK_a}_{solv}$, using the relation

$$pK_a = \frac{\Delta G^{\circ,pK_a}_{solv}}{\ln(10)RT} \quad (5)$$

where R is the gas constant and T is the temperature. The free energy of deprotonation for a molecule AH is defined to be the free energy change associated with the following reaction:

$$AH_{solv} \rightarrow A^-_{solv} + H^+_{solv} \quad (6)$$

Analogous to calculations of the reduction potentials, the calculation of $\Delta G^{\circ,pK_a}_{solv}$ can be performed with structures optimized in the gas phase using a Born−Haber thermodynamic cycle or with structures optimized in solution. In the Born−Haber cycle, $\Delta G^{\circ,pK_a}_{solv}$ is expressed in terms of the free energy of deprotonation in the gas phase, $\Delta G^{\circ,pK_a}_{gas}$, and the solvation free energies of the acid, conjugate base, and proton, $\Delta G^{\circ}_{s}(AH)$, $\Delta G^{\circ}_{s}(A^-)$, and $\Delta G^{\circ}_{s}(H^+)$, respectively:

$$\Delta G^{\circ,pK_a}_{solv} = \Delta G^{\circ,pK_a}_{gas} + \Delta G^{\circ}_{s}(A^-) - \Delta G^{\circ}_{s}(AH) + \Delta G^{\circ}_{s}(H^+) \quad (7)$$

where $\Delta G^{\circ,pK_a}_{gas}$ is calculated from eq 4.[36] Alternatively, $\Delta G^{\circ,pK_a}_{solv}$ can be calculated with structures optimized in solution using the analogue of eq 4 with thermodynamic quantities obtained in solution.

Analogous to the electron in the reduction potentials, the free energy associated with the proton will contribute to $\Delta G^{\circ,pK_a}_{solv}$. As for the reduction potentials, the contribution from the proton will cancel exactly when the pK_a is calculated relative to the known pK_a of a related system and is only required for the calculation of absolute pK_a's.[37] When it is required, the contribution from the proton to $\Delta G^{\circ,pK_a}_{gas}$ can be calculated for an ideal gas with Boltzmann statistics, leading to $G^{\circ}_{gas}(H^+) = -6.28$ kcal/mol.[12] The solvation free energy of a proton, $\Delta G^{\circ}_{s}(H^+)$, in various solvents has been debated in the literature and has been determined to be −264.0 or −258.3 kcal/mol for water or acetonitrile, respectively.[35,38−41] Different conventions have led to a variety of estimations of the absolute potential of the half-cell reaction $^1/_2H_{2,gas} \rightarrow H^+_{aq} + e^-_{gas}$, adding to the uncertainty in the exact value.[29,34,35,38,42−44]

Finally, the issue of standard states must be considered in calculations of reduction potentials and pK_a's when the electron and proton are treated explicitly.[41] For calculations of the free energies of solvation, the change in standard-state concentration upon going from the gas phase (1 atm or 1 bar) to solution (1 M) should be included by adding a constant that has been determined to be −1.9 kcal/mol at 298.15 K.[12,41] Given all of the considerations discussed in this subsection, it is advantageous to calculate *relative* reduction potentials and *relative* pK_a's to ensure that the free energies of the electron and proton, as well as the effect of standard states, will cancel.

B. Reference Reactions. As mentioned above, calculation of the reduction potentials and pK_a's relative to a reference system with a known value often provides more quantitatively accurate results.[15−17,45] An example of the use of a reference reaction for the calculation of a reduction potential is depicted in Scheme 2. In this case, the reaction of interest is the

Scheme 2. Calculation of Reduction Potentials Using a Reference

$Ox + e^- \rightarrow Red$	$-FE^{\circ}$
$Red_{ref} \rightarrow Ox_{ref} + e^-$	FE°_{ref}
$Red_{ref} + Ox \rightarrow Ox_{ref} + Red$	ΔG°_{r}

reduction of Ox to Red, and the reference reaction is the reduction of Ox_{ref} to Red_{ref}. The reduction potential for the system of interest can be expressed as

$$E^{\circ} = \frac{-\Delta G^{\circ}_{r}}{F} + E^{\circ}_{ref} \quad (8)$$

where ΔG°_{r} is the free energy change associated with the reaction

$$Red_{ref} + Ox \rightarrow Ox_{ref} + Red \quad (9)$$

and E°_{ref} is the reduction potential of the reference species. The quantity ΔG°_{r} is calculated with quantum chemistry methods, and E°_{ref} is typically known from experimental measurements.

dx.doi.org/10.1021/ic5002896 | Inorg. Chem. 2014, 53, 6427−6443

The choice of the experimental value for E°_{ref} determines the type of reduction potential that will be calculated within this reference framework. In cyclic voltammetry, current peaks are often reported as $E_{1/2}$, or the half-wave potential, which is the arithmetic average of the current peak maximum and minimum positions for a reversible reaction. Typically, the half-wave potential closely corresponds to the standard reduction potential, E°. For peaks that are not perfectly reversible, the current peaks are often reported as E_p, which is the position of the maximum (minimum) current of the cathodic (anodic) sweep, or as $E_{p/2}$, which is the position at which the cathodic (anodic) sweep is half of its maximum (minimum) current.[46] The type of measurement used to determine E°_{ref} will govern the type of value that will be calculated for the species of interest (e.g., to calculate E_p rather than E°, E°_{ref} should be replaced with $E_{p,ref}$ of an irreversible reaction in eq 8).

Usually E°_{ref} has been measured with respect to a particular reference electrode, and E° is calculated with respect to the same reference electrode without requiring an explicit treatment of the electrode potential. Moreover, as discussed above, calculation of the free energy associated with the electron is not required because this contribution cancels exactly. This procedure can yield highly accurate calculated reduction potentials when the reference species is suitably close to the species of interest because of cancellation of the errors within the quantum chemistry calculations as well as these other factors.

A reference reaction can be used in a similar way in the context of pK_a calculations. In this case, the reaction of interest is the deprotonation of AH to A^-, and the reference reaction is the deprotonation of AH_{ref} to A^-_{ref}. The pK_a for the system of interest can be expressed as

$$pK_a(AH) = \frac{\Delta G^\circ_r}{\ln(10)RT} + pK_a(ref) \quad (10)$$

where ΔG°_r is the free energy change associated with the reaction

$$A^-_{ref} + AH \rightarrow AH_{ref} + A^- \quad (11)$$

and pK_a(ref) is the known pK_a of the reference species. This procedure avoids the errors associated with the free energy of the proton because this contribution cancels exactly. In addition, the errors in the quantum chemistry calculations will also cancel if the reference species is suitably close to the species of interest.

Reference reactions can also be useful in cases where ligand dissociation occurs. A common occurrence in the calculation of reduction potentials of transition metal complexes is that an axial solvent ligand dissociates upon reduction.[47] In this case, the reduction reaction shown in eq 2 becomes

$$Ox{-}L_{solv} + e^- \rightarrow Red_{solv} + L_{solv} \quad (12)$$

The treatment of the ligand L, which dissociates upon reduction, with quantum chemistry methods is complicated by basis set superposition error,[48] as well as fundamental issues associated with the calculation of the solvation free energy associated with moving a solvent molecule from the gas phase to its own pure liquid phase.[41] These complications can be avoided by using a reference reaction that also experiences ligand loss upon reduction. The analogue of eq 9 that arises in this treatment is

$$Red_{ref} + Ox{-}L \rightarrow Ox{-}L_{ref} + Red \quad (13)$$

where all quantities are defined in the same manner as in Scheme 2 except that a ligand is bound to the oxidized species of both the system of interest and the reference system. In this case, the ligand as well as the electron cancels in the overall reaction, so the ligand does not need to be treated explicitly. Note that this cancellation occurs only when the same ligand is lost in the reference reaction as in the reaction of interest. Moreover, the cancellation of errors is expected to be best when the metal center losing the ligand is also the same in both reactions.

When suitable references are used, the accuracy of quantum chemistry calculations is ~0.1 V for reduction potentials and ~1−2 pK_a units.[15−17,45] Obtaining this level of accuracy without taking advantage of the cancellation of errors with reference reactions is extremely challenging. As discussed above, when reference reactions are not used, errors are associated with the free energy of the electron or proton, as well as the reduction potential of the electrode. Additional errors are associated with the level of electronic structure, such as limitations in the basis sets and the functionals in density functional theory (DFT) and the harmonic approximation used to calculate the zero-point energy and entropic contributions to the free energies. Further errors are associated with the treatment of solvation, which often relies on a polarizable continuum model that neglects specific hydrogen bonding between solvent and solute molecules. Many of these errors at least partially cancel when reference reactions are used.

C. Quantum Chemistry Methods. Molecular electrocatalysts are typically studied with DFT[49,50] because higher levels of theory, such as coupled cluster methods, are computationally intractable. A wide range of functionals, including hybrid functionals that contain a portion of Hartree−Fock exchange, are available for DFT calculations. Various studies have assessed the accuracies of the available functionals for calculating reduction potentials and pK_a's.[11,51] Some popular functionals for transition metal electrocatalysts are B3LYP, BP86, B3P86, PBE, TPSSh, M06L, and ωB97XD.[52] For moderately sized molecular electrocatalysts (~50−100 atoms), these functionals are often used in conjunction with a double-ζ basis set, such as 6-31G, or adding polarization, 6-31G*.[53−55] Triple-ζ basis sets can be used for smaller catalysts, and diffuse basis functions can be added for anionic systems. Moreover, additional polarization can be added for specific key atoms, such as the transferring proton. Often pseudopotentials are used for transition metal centers to decrease the computational cost.[56]

Typically, the solvent is treated with a polarizable continuum model, in which the solvent is represented as a homogeneous dielectric continuum.[57−60] The advantage of such models is that they include the key electrostatic interactions between the solvent and solute, as well as the entropic contributions from the solvent, in a computationally tractable manner. An alternative approach is to immerse the solute in a box of explicit solvent molecules and calculate the free energy changes with molecular dynamics methods.[61,62] This approach is more computationally expensive and relies on accurate force fields for the intermolecular interactions, as well as adequate conformational sampling. A disadvantage of polarizable continuum models is that they neglect the specific hydrogen-bonding interactions between solvent and solute molecules. In some cases, a polarizable continuum model can be used in conjunction with a small number of explicit solvent molecules positioned around the catalyst.[63] This type of combined

dx.doi.org/10.1021/ic5002896 | Inorg. Chem. 2014, 53, 6427−6443

method includes specific hydrogen-bonding effects, but unfortunately the results are strongly dependent on the initial positions of the solvent molecules because the system can become stuck in local minima. In certain cases, however, key solvent molecules must be included explicitly in the system. For example, axial solvent ligands for metal-based catalysts should be included explicitly because they are interacting directly with the metal center. Thus, a reliable approach is to include only the key solvent molecules, such as axial solvent ligands,[14,16,32] in conjunction with a polarizable continuum model.

III. THERMODYNAMIC SCHEMES, POURBAIX DIAGRAMS, AND LINEAR CORRELATIONS

The calculated thermodynamic properties for all of the individual ET and PT steps can be combined to generate a thermodynamic scheme depicting the free energy relations among all possible species (i.e., all physically meaningful oxidation and protonation states). This information can be used to generate thermodynamic reaction pathways, which provide insight into the thermodynamically favorable mechanisms. For completeness, all possible mechanisms for the ET and PT steps should be considered. For example, a reaction involving two ET and two PT steps could occur by the following mechanisms: ET−PT−ET−PT, PT−ET−PT−ET, ET−ET−PT−PT, PT−PT−ET−ET, and so forth. For each possible mechanism, the free energy associated with each step is plotted along the proposed reaction pathway. Typically, the electrons and protons are assumed to be obtained from an electrode and an acid, respectively. The free energies will depend on the reference electrode and the applied overpotential, as well as the pK_a of the acid. A comparison of the various reaction pathways will help to identify the thermodynamically favorable pathways, which are either entirely downhill in free energy or reasonably flat, avoiding low sinks in which the system could become trapped and high rises that must be surmounted. An example of calculating the thermodynamic reaction pathways and identifying the thermodynamically favorable mechanisms will be given in section V for cobaloximes.

Another useful tool for envisioning the relationship between ET and PT reactions is the Pourbaix diagram, which depicts the most thermodynamically stable species for a given reduction potential and pH value.[64] The Pourbaix diagram for a specific nickel-based electrocatalyst is shown in section VII. The horizontal and vertical lines correspond to the reduction potentials and pK_a's, respectively, of the various species. Crossing a horizontal line toward a more negative potential indicates that the complex becomes reduced, while crossing a vertical line toward a lower pH indicates that the complex becomes protonated. Diagonal lines are drawn when changes to both the oxidation and protonation states occur, and the slope reflects the ratio of protons to electrons involved in this process. Specifically, according to the Nernst equation, an electron/proton reaction given as

$$\mathrm{Ox} + n\mathrm{e}^- + m\mathrm{H}^+ \rightleftarrows [\mathrm{Red(H)}_m]^{m-n} \qquad (14)$$

leads to a slope of $-\ln(10)RTm/(nF) = -(m/n)59$ mV/pH at 298.15 K. The effect of a greater degree of protonation on the reduction potential can be described as a Nernstian response, which follows a diagonal boundary in a Pourbaix diagram. Catalyst design can incorporate this effect by allowing for ligand protonation, thereby making reduction potentials less negative in an effort to lower the required overpotential. The experimental conditions can be reversibly modified (i.e., applying a greater overpotential or using a stronger acid) to move along the diagonal boundaries, without changing the overall mechanism. These diagonal boundaries eventually terminate at new horizontal and/or vertical lines in regions where either the electrons or protons are no longer transferring. As mentioned above, an example of a Pourbaix diagram and a Nernstian response is given in section VII for a nickel-based catalyst with pendant amines.

Originally, the Pourbaix diagram was devised for only aqueous environments.[64] For nonaqueous solvents, pH is not a well-defined quantity, and the label of pH on the x-axis of a Pourbaix diagram implicitly refers to the pK_a of an acid in the specified solvent. Thus, for nonaqueous solvents, the Pourbaix diagram depicts the most thermodynamically stable species for a given reduction potential in the presence of an acid with a given pK_a in that solvent. According to this interpretation, Pourbaix diagrams can be generated for nonaqueous as well as aqueous environments.

While thermodynamic schemes and Pourbaix diagrams pertain to one particular complex, reduction potentials and pK_a's of a series of related complexes can also be linearly correlated.[15,18,65] For example, the complexes could be modified by adding electron-withdrawing or electron-donating substituents to the ligands. Modification of a metal-based electrocatalyst that results in a less negative reduction potential typically also results in a lower pK_a of the metal center. This relation is based on simple electrostatics, namely, that a metal center more receptive to the addition of an electron is likely to be less receptive to the addition of a proton. The degree to which the reduction potential becomes less negative and the pK_a decreases is related to the slope of the line correlating these two properties over a range of reduction potentials and acid strengths. In some cases, the reduction potentials and pK_a's can be linearly correlated to a property of the ligands, such as the Hammett constant, which is a measure of the electron-withdrawing or electron-donating character of the ligand.[18,65,66] An example of these types of linear correlations will be given in section V for cobaloximes. In addition, more complicated correlations among the thermodynamic properties involving protonation of the ligands as well as the metal center have been observed for the nickel-based catalysts with pendant amines, as will be discussed in section VII. Such correlations are powerful tools in catalyst design, allowing computational studies to predict the properties of electrocatalysts that have not yet been synthesized.

IV. NONINNOCENT LIGANDS IN MOLECULAR ELECTROCATALYSTS

The ligands on molecular electrocatalysts are often perceived as noninnocent in that they serve as protonation and reduction sites. In this section, we discuss ligand protonation, illustrating this effect with cobalt dithiolenes, and ligand reduction. The issue of spin states is also discussed in the subsection on ligand reduction.

A. Ligand Protonation. The protonation of ligands serves several different mechanistic roles in molecular electrocatalysis. First, the ligand can directly donate the proton in a chemical reaction such as the production of H_2. Second, the ligand can serve as a proton relay to shuttle the proton to the metal center to generate a metal hydride that could be active in a chemical reaction such as H_2 production. Third, ligand protonation can

dx.doi.org/10.1021/ic5002896 | Inorg. Chem. 2014, 53, 6427−6443

shift the reduction potential in a manner that decreases the overpotential required for a catalytic reaction because the complex is more easily reduced as a result of the additional positive charge, as discussed in the previous section in terms of a Nernstian response. We will discuss the role of ligand protonation for H_2 production in the context of cobaloximes in section V and the nickel-based catalysts with pendant amines in section VII. Here we provide an example of how ligand protonation impacts the reduction potentials and explains anomalous behavior for a series of cobalt dithiolene catalysts.

The series of cobalt dithiolenes depicted in Chart 1 was studied photochemically and electrochemically as H_2 evolution

Chart 1. Cobalt Dithiolene Complexes

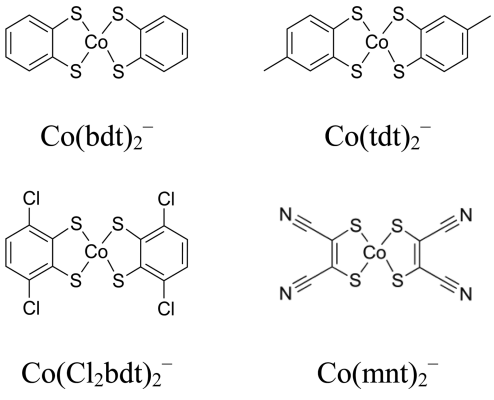

catalysts in 1:1 (v/v) acetonitrile/water.[67,68] As expected, the $Co^{III/II}$ reduction potential is least negative for the complex with the most electron-withdrawing substituents, $Co(mnt)_2$ (mnt = maleonitrile-2,3-dithiolate), and most negative for the complex with the most electron-donating substituents, $Co(tdt)_2$ (tdt = toluene-3,4-dithiolate). Moreover, the photocatalytic activity of these complexes follows the same order, where $Co(mnt)_2$ exhibits the largest turnover frequency. The required electrocatalytic overpotentials follow the same trend, with the notable exception that $Co(mnt)_2$ operates at the most negative potential rather than the least negative potential as expected. This observation suggests that $Co(mnt)_2$ is the least active electrocatalyst in the series.

Calculations of the reduction potentials and relative pK_a's provide an explanation for this anomalous behavior in terms of ligand protonation.[69] Specifically, the calculations indicate that, after the initial $Co^{III/II}$ reduction, one fewer sulfur atom is protonated in the $Co(mnt)_2$ complex than in the other three complexes in the series. Because of the lower degree of ligand protonation, the subsequent $Co^{II/I}$ reduction step occurs at the most negative potential for $Co(mnt)_2$. Moreover, the calculated relative pK_a's also provide mechanistic insight, suggesting that it is thermodynamically favorable for one of the protons on the ligands to transfer intramolecularly to the cobalt center after the two reduction steps, forming the key cobalt hydride intermediate for H_2 evolution.

B. Ligand Reduction. In some molecular electrocatalysts, a ligand rather than the metal center can serve as the electron acceptor upon reduction. Understanding this aspect of these catalysts is important for interpreting the cyclic voltammogram peaks. Ligand reduction has structural implications, such as preferred metal geometries, and mechanistic implications, namely, in determining the preferred protonation sites to be either the metal center or the ligands. Electronic structure calculations can be used to identify the electron acceptor upon reduction. Specifically, the localization of unpaired electrons can be analyzed via the spin density in quantum chemistry calculations. For systems with a single unpaired electron, this type of analysis can be used to determine whether the unpaired electron is localized on the ligand or the metal center. In some cases, even when the system has an even number of electrons, an unpaired electron may be localized on the ligand, while another unpaired electron is localized on the metal center, leading to an open-shell singlet or a triplet. Alternatively, a triplet state could correspond to two unpaired electrons on the ligands or the metal center.

Quantum chemistry calculations can be used to investigate all of these possible scenarios, but special care should be taken for these types of calculations. When considering open-shell complexes, DFT and other self-consistent-field methods can often find local minima, leading to geometries and spin densities that do not correspond to the most stable state. Furthermore, when considering multiple unpaired electrons, the problem is inherently multireference, and DFT is a single-reference method that lacks static correlation. For this reason, DFT is not always reliable for these types of calculations, and a range of different exchange-correlation functionals should be examined to provide some degree of validation of the results. In addition, solvation can affect the stability of certain high-spin states, so optimization in solvent may be necessary to correctly predict the energetic ordering of different spin states. A previous Forum of *Inorganic Chemistry* addresses redox-active ligands,[70,71] including metal dithiolenes.[72]

V. COBALOXIMES FOR H_2 PRODUCTION

In this section, we illustrate the methods and concepts described in the previous sections with an example of cobaloximes, $Co(dRgBF_2)_2$, which are depicted in Chart 2 for

Chart 2. Cobaloxime Catalysts

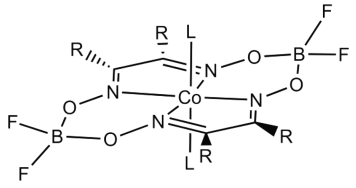

R = CN, CF_3, Cl, H, C_6H_5, CH_3, OCH_3, OH, NH_2
L = solvent

a series of substituents R. Several possible mechanisms for H_2 evolution catalyzed by cobaloximes are depicted in Scheme 3.[16,65] Pathway 1 (shown in green) is characterized by evolving H_2 from a cobalt(III) hydride intermediate, while pathway 2 (shown in purple) is characterized by evolving H_2 from a cobalt(II) hydride intermediate. Both mechanisms can be described as proceeding monometallically (A), in which a single cobalt hydride intermediate interacts with an external acid to form molecular H_2, or bimetallically (B), in which two cobalt hydride intermediates interact to form molecular H_2.

Figure 1 depicts the free energy reaction pathway diagrams for $Co(dmgBF_2)_2$ (dmg = dimethylglyoxime), shown in Chart 2 (R = CH_3), in acetonitrile with tosic acid (pK_a = 8.0 in acetonitrile). These free energy diagrams are plotted at an electrode potential equal to the $Co^{II/I}$ reduction potential, corresponding to typical experimental conditions for these

dx.doi.org/10.1021/ic5002896 | Inorg. Chem. 2014, 53, 6427−6443

Scheme 3. Monometallic (A) and Bimetallic (B) Pathways for Cobaloxime Catalysts

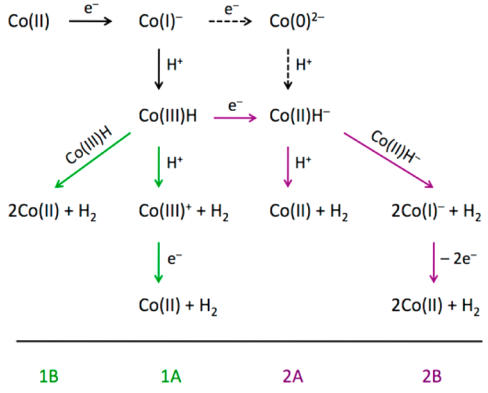

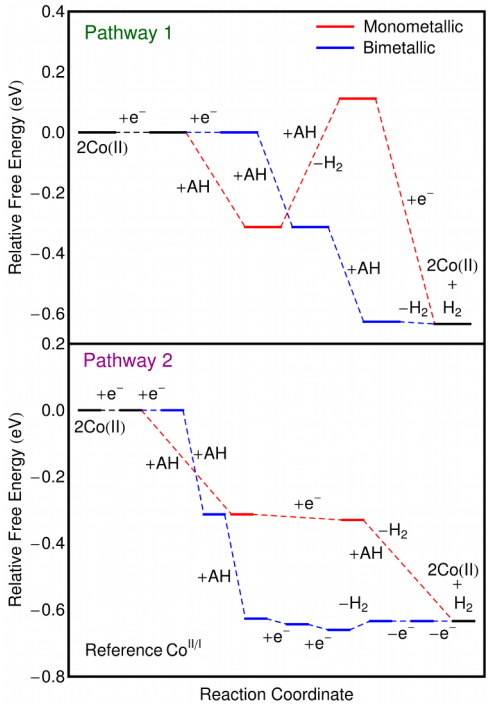

Figure 1. Free energy diagrams for $Co(dmgBF_2)_2$ (Chart 2; R = CH_3) in acetonitrile for the pathways shown in Scheme 3: pathway 1 (upper frame) and pathway 2 (lower frame) with the monometallic (red) and bimetallic (blue) mechanisms. Black lines denote states that are applicable to both monometallic and bimetallic pathways. Relative free energies for half-reactions corresponding to ET are calculated with respect to the $Co^{II/I}$ couple in acetonitrile. In this diagram AH is $TsOH{\cdot}H_2O$ (pK_a = 8.0). The free energy barriers are not shown. The figure was modified from a related figure in ref 16.

electrocatalysts[73,74] and resulting in no free energy change for $Co^{II/I}$ reduction. For the monometallic mechanisms (red paths), pathway 2A, which is entirely downhill in Figure 1, is the thermodynamically preferred mechanism. For the bimetallic mechanisms (blue paths), pathways 1B and 2B, which correspond to reactions between two $Co^{III}H$ and two $Co^{II}H^-$ intermediates, respectively, are both thermodynamically favorable in that they are downhill for almost every elementary step with only a few minor increases in free energy. Because $Co^{III}H$ is neutral and $Co^{II}H^-$ is anionic, however, pathway 1B is predicted to be more favorable than pathway 2B because of the larger electrostatic work term required to bring together two anions in solution for reaction.

We also considered a third pathway (shown with dashed lines in Scheme 3), which involves an additional reduction to Co^0, followed by protonation to generate a cobalt(II) hydride intermediate. However, we found that the $Co^{I/0}$ reduction potential is so negative that this mechanism is thermodynamically unfavorable under typical experimental conditions.[75,76] On the other hand, this pathway could become favorable if a sufficiently high overpotential is applied to favor $Co^{I/0}$ reduction, and a sufficiently weak acid is used to disfavor Co^I protonation. In general, the thermodynamically favorable pathway can be changed by altering the experimental conditions, such as the applied overpotential, acid strength, and acid concentration.

In cyclic voltammograms of $Co(dmgBF_2)_2$ with tosic acid in acetonitrile, a peak at ca. −1 V vs SCE was tentatively identified as the $Co^{III/II}H$ reduction potential.[74] We calculated the reduction potential of $Co^{III/II}H$ to be −0.53 V vs SCE in acetonitrile and the reduction potential of $Co^{II/I}H$ to be somewhat more negative than −1 V vs SCE in acetonitrile.[16] On the basis of these calculations, we suggested a reassignment of the experimentally observed peak at ca. −1 V vs SCE to the $Co^{II/I}H$ reduction potential.[16] Similar conclusions were reached by Muckerman and Fujita based on independent calculations.[29]

This reassignment has mechanistic implications because the monometallic pathway 2A requires the reduction of $Co^{III}H$. On the basis of the initial peak assignment, the $Co^{III/II}H$ reduction would require a potential of ca. −1 V vs SCE and hence would be thermodynamically unfavorable at the $Co^{II/I}$ reduction potential, which is −0.55 V vs SCE in acetonitrile. This interpretation, which is based on the initial peak assignment, suggests that the monometallic pathway is not viable under typical experimental conditions. According to our calculations, however, the $Co^{III/II}H$ reduction potential is −0.53 V vs SCE in acetonitrile and therefore is thermodynamically favorable at the $Co^{II/I}$ reduction potential, as illustrated in Figure 1. This interpretation, which relies on the peak reassignment, supports the monometallic pathway 2A. Further support for the monometallic pathway 2A was later provided by experiments that controlled protonation with a photoacid.[77]

Although the peak reassignment discussed above indicates that monometallic pathway 2A should not be ruled out on the basis of thermodynamic arguments, the bimetallic pathway 1B for $Co(dmgBF_2)_2$ has not been ruled out either. Either monometallic pathway 2A or bimetallic pathway 1B could be favored under different experimental conditions. For example, the monometallic pathway would be favored for a high concentration of acid relative to catalyst. This study illustrates how calculations can assist in the assignment of cyclic voltammogram peaks and provide mechanistic insight.

Calculations have also been used to predict substituent effects on the electrochemical and catalytic properties of cobaloximes. Linear correlations were found between the reduction potentials and the pK_a's for the series of cobaloximes depicted in Chart 2.[65] As shown in Figure 2, linear correlations were also found between these properties and the Hammett constant σ_p, which quantifies the electron-donating or electron-withdrawing strength of the substituent.[66] More strongly electron-withdrawing (electron-donating) substituents lead to more positive (negative) reduction potentials and more negative (positive) pK_a's. From the slopes and intercepts of each linear correlation, we can predict all of these reduction

dx.doi.org/10.1021/ic5002896 | Inorg. Chem. 2014, 53, 6427−6443

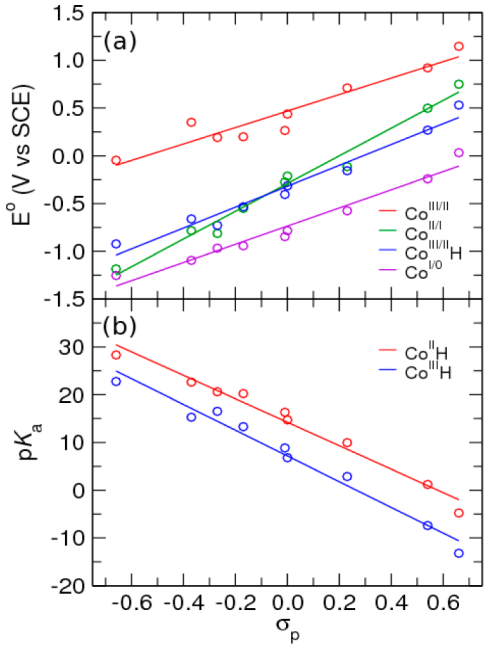

Figure 2. (a) Calculated reduction potentials and (b) calculated pK_a's for Co(dRgBF$_2$)$_2$ as functions of the Hammett constants for a series of substituents R = −NH$_2$, −OH, −OCH$_3$, −CH$_3$, −C$_6$H$_5$, −H, −Cl, −CF$_3$, −CN (Chart 2). The figure was reproduced with permission from ref 65. Copyright 2011 American Chemical Society.

potentials and pK_a's for a given cobaloxime if the Hammett constant of the substituent or only one of these quantities is known. Furthermore, the crossing of the blue and green lines in Figure 2a illustrates that the Co$^{III/II}$H and Co$^{II/I}$ reduction potentials are very similar for mildly electron-donating substituents such as methyl groups. This observation is consistent with the reassignment of the peak at ca. −1 V vs SCE for Co(dmgBF$_2$)$_2$ in acetonitrile from Co$^{III/II}$H to Co$^{II/I}$H because the Co$^{III/II}$H peak is likely to be obscured by the more prominent Co$^{II/I}$ peak. These linear correlations also provide a prediction that the two peaks will be separated for cobaloximes with substituents that are more electron-withdrawing or electron-donating (i.e., for more positive or negative Hammett constants).

Upon reanalysis of the cyclic voltammograms of Co(dpgBF$_2$)$_2$ (dpg = diphenylglyoxime) in acetonitrile in ref 73, we discovered a small irreversible peak that appears at ca. −0.5 V vs SCE in the presence of HBF$_4$ (pK_a = 0.1 in acetonitrile). This peak is more negative than the catalytic peak that occurs at the Co$^{II/I}$ reduction potential of −0.28 V vs SCE. On the basis of our prediction that the Co$^{III/II}$H peak will shift negative of the Co$^{II/I}$ peak with more electron-withdrawing substituents,[65] we assign this small irreversible peak to the Co$^{III/II}$H couple. This assignment is consistent with our calculated value of $E°$(Co$^{III/II}$H) = −0.40 V vs SCE in acetonitrile for Co(dpgBF$_2$)$_2$.[16] Because Co^{III}H cannot be reduced to Co^{II}H at an applied potential of −0.28 V vs SCE, the H$_2$ evolution mechanism cannot follow pathway 2 under these experimental conditions (i.e., for this applied potential). Except in the presence of very strong acids, the calculations suggest that pathway 1A is also thermodynamically unfavorable.[16] This analysis implies that the most thermodynamically favorable pathway for H$_2$ production by Co(dpgBF$_2$)$_2$ under moderate acidic conditions at an applied potential corresponding to the Co$^{II/I}$ reduction potential is the bimetallic pathway 1B. Thus, the monometallic mechanism may be favorable for methyl-substituted cobaloximes but not for phenyl-substituted cobaloximes under certain experimental conditions.

The effects of ligand modification and protonation on metal oximes have also been investigated both experimentally and theoretically.[78−80] For example, one or both of the O−BF$_2$−O bridges in Co(dRgBF$_2$)$_2$ can be replaced by an O−H−O bridge or by propane. Experiments suggest that metal oximes with two O−H−O bridges degrade in acidic solution,[81,82] so these complexes were not studied extensively as H$_2$ evolution catalysts. Calculations for complexes with a single O−H−O bridge indicate that ligand protonation is likely to occur at this bridge and that a ligand-protonated cobalt(III) hydride intermediate may be formed along the H$_2$ production pathway in the presence of sufficiently strong acid.[80] Moreover, the calculated Co$^{II/I}$ reduction potentials exhibit a Nernstian response, where the reduction potential becomes significantly less negative upon protonation at the O−H−O bridge. The anodic shift due to protonation at the O−H−O bridge was found to be greater than that due to replacement of the O−H−O bridge with the more electron-withdrawing O−BF$_2$−O bridge. Thus, these studies suggest that asymmetric cobaloxime complexes containing a single O−H−O bridge may be effective H$_2$ evolution electrocatalysts with relatively low overpotentials. These experimental and theoretical studies were performed in both water and acetonitrile, and metal oximes with nickel and iron centers were also investigated.[78,80,83−85] Overall, these calculations provide insight into the relative effects of ligand modification and protonation, as well as metal substitutions, in two different solvents. Such insights are useful for the design of more effective catalysts for H$_2$ production.

VI. KINETIC ASPECTS OF MOLECULAR ELECTROCATALYSTS

In addition to the thermodynamic aspects discussed in the previous sections, the kinetics of the various steps in the reaction pathways also play an important role in molecular electrocatalysis. To examine the kinetics, we need to calculate the rate constants for PT, ET, and concerted PCET, denoted EPT. Other steps, such as intramolecular isomerizations, may also play a kinetic role, and barriers for these types of processes must also be examined to obtain a complete picture of the catalytic cycle. In this section, we briefly summarize the methods to calculate the rate constants for PT, ET, and EPT. The reader is referred to other sources for more detailed discussions of these topics.

A. Proton Transfer. The rate constant for a single PT reaction can be calculated using data obtained with quantum chemistry methods such as DFT. The geometries of the transition state and minima associated with PT can be determined with optimization techniques, and the vibrational frequencies of the normal modes can be used to calculate the zero-point energy and entropic contributions to the free energies.[17,86,87] These calculations can include solvent effects using a polarizable continuum model. The resulting free energy barrier $\Delta G^{‡}$ can be used to estimate a rate constant for PT using the standard transition state theory rate constant expression

$$k_{TST}^{PT} = \frac{k_B T}{h} \exp(-\Delta G^{‡}/k_B T) \quad (15)$$

dx.doi.org/10.1021/ic5002896 | Inorg. Chem. 2014, 53, 6427−6443

where k_B is Boltzmann's constant and h is Planck's constant. This expression neglects dynamical barrier recrossings and hydrogen tunneling effects.[22]

Several challenges arise in these types of calculations. The calculation of the free energy barrier is typically more straightforward for intramolecular PT than for intermolecular PT. For the latter, geometry optimizations of the hydrogen-bonded complex comprised of the catalyst and the acid may be difficult because of the relatively weak intermolecular interactions. Moreover, a full description of intermolecular PT requires the equilibrium constant associated with forming this hydrogen-bonded complex, which is difficult to calculate accurately for technical reasons such as basis set superposition error[48] and treatment of the rotational and translational degrees of freedom in the partition function used to calculate the entropic contributions.[31] An issue that pertains to both intra- and intermolecular PT is the treatment of solvation with polarizable continuum models because hydrogen bonding between solvent molecules and the catalyst may play a role. An alternative approach is to calculate the free energy barrier with mixed quantum mechanical/molecular mechanical molecular dynamics simulations of the catalyst in a box of explicit solvent molecules. However, this approach depends on the accuracy of the molecular mechanical force field and requires sufficient conformational sampling.

Another important issue that may arise for PT reactions is that hydrogen tunneling effects could be important.[22] In such cases, hydrogen tunneling can be included using a dynamical method such as variational transition state theory with semiclassical tunneling contributions,[88,89] path integral formulations,[90,91] or grid-based approaches in which the transferring hydrogen nucleus is treated quantum mechanically.[92] Moreover, analytical rate constant expressions that include hydrogen tunneling effects for PT reactions are available in certain limits.[21,22]

B. Electron Transfer. The rate constants for ET can be calculated in the framework of Marcus theory.[93] The free energy profiles for the two diabatic states corresponding to the electron localized on the donor or acceptor, respectively, are depicted schematically in Figure 3. In the nonadiabatic limit for electrochemical ET, the anodic and cathodic rate constants are

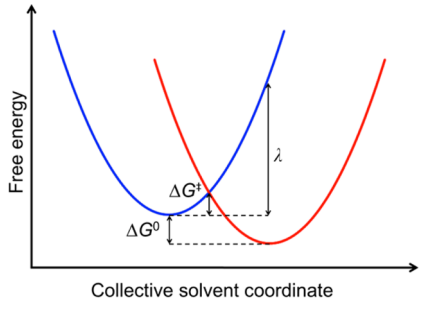

Figure 3. Free energy curves associated with the diabatic electronic states along the collective solvent coordinate for an asymmetric homogeneous ET reaction. The blue and red curves correspond to the diabatic states with the electron localized on the donor and acceptor, respectively. The reorganization energy, λ, reaction free energy, ΔG°, and free energy barrier, $\Delta G^\ddagger$, are indicated. According to Marcus theory, the intrinsic free energy barrier is $\Delta G^\ddagger = \lambda/4$, corresponding to $\Delta G^\circ = 0$. The figure was adapted from ref 22.

$$k_a^{ET}(\eta) = \frac{(V^{el})^2}{\beta'\hbar}\sqrt{\frac{\pi}{k_B T\lambda}}\rho_M \int d\varepsilon\,[1 - f(\varepsilon)]\exp\left[-\frac{(\varepsilon - e\eta + \lambda)^2}{4\lambda k_B T}\right]$$

$$k_c^{ET}(\eta) = \frac{(V^{el})^2}{\beta'\hbar}\sqrt{\frac{\pi}{k_B T\lambda}}\rho_M \int d\varepsilon\, f(\varepsilon)\exp\left[-\frac{(-\varepsilon + e\eta + \lambda)^2}{4\lambda k_B T}\right] \quad (16)$$

where $f(\varepsilon)$ is the Fermi distribution function for the electronic states in the electrode, ρ_M is the density of states at the Fermi level, which is assumed to be a constant in the vicinity of the Fermi level, V^{el} is the electronic coupling, β' is a parameter of magnitude ~1−3 Å^{-1} representing the exponential decay of the electronic coupling with the distance between the molecule and the electrode, and λ is the reorganization energy defined in Figure 3. According to Marcus theory,[94] the intrinsic free energy barrier for ET is $\lambda/4$, implying that the reorganization energy is one of the most important quantities to calculate. In general, the reorganization energy is the sum of inner-sphere (solute) and outer-sphere (solvent) contributions.

The inner-sphere reorganization energy is associated with the solute rearrangement upon ET. This quantity can be calculated with the "four-point method"[95] given by the following expression:

$$\lambda_i = \frac{1}{2}[E_{ox}(R_{eq}^{red}) - E_{ox}(R_{eq}^{ox}) + E_{red}(R_{eq}^{ox}) - E_{red}(R_{eq}^{red})] \quad (17)$$

Here R_{eq}^{ox} and R_{eq}^{red} are the optimized equilibrium geometries of the oxidized and reduced species, respectively, and E_{ox} and E_{red} are the energies of the oxidized and reduced states, respectively, evaluated at the designated geometry. Thus, the calculation of the inner-sphere reorganization energy requires the geometry optimization of both the reduced and oxidized species and single-point calculations for each geometry in the complementary oxidation state.

The outer-sphere or solvent reorganization energy reflects the change in solvent polarization upon ET. This quantity can be calculated using dielectric continuum theory, where the solvent is represented as a homogeneous dielectric medium. An analytical expression for the solvent reorganization energy has been derived for a model comprised of a point charge in a sphere of radius a located a distance d from the electrode surface and immersed in a solvent with static dielectric constant ε_0 and optical dielectric constant ε_∞. The solvent reorganization energy for this model is[96,97]

$$\lambda_s = \frac{(\Delta q)^2}{2}\left(\frac{1}{\varepsilon_\infty} - \frac{1}{\varepsilon_0}\right)\left(\frac{1}{a} - \frac{1}{2d}\right) \quad (18)$$

where Δq is the change in charge upon ET. The radius of the sphere can be determined from the volume of the molecular cavity obtained with a polarizable continuum model. The distance between the molecule and the electrode surface can be determined from the outer Helmholtz plane or, in certain cases, the inner Helmholtz plane. The inner and outer Helmholtz planes are defined in terms of the radii of the solvent molecules and the solvated electrolyte ions.[98,99]

Recently, a computational approach has been implemented for calculating the electrochemical solvent reorganization

dx.doi.org/10.1021/ic5002896 | Inorg. Chem. 2014, 53, 6427−6443

energies using electronic structure methods in conjunction with a polarizable continuum model.[100] This approach accounts for the effects of the molecular charge redistribution in a molecular-shaped cavity, as well as the slow and fast time scale solvent responses and the effects of the electrode. The resulting electrochemical solvent reorganization energies were shown to be similar to those obtained from the analytical expression in eq 18 for the molecules studied, as long as the radius a in eq 18 was determined by the volume of the molecular cavity obtained from the polarizable continuum model.[100] Moreover, the calculated reorganization energies were in reasonable agreement with experimental measurements for the systems studied. An alternative approach for calculating the solvent reorganization energy is to perform molecular dynamics simulations of the molecule immersed in a box of explicit solvent molecules.[61,62] However, it is challenging to accurately account for the electrode response with such an approach.[101−105]

In addition to the reorganization energy, another important parameter in the ET rate constant expression is the electronic coupling. A variety of computational methods have been developed to calculate the electronic coupling between a molecule and an electrode,[106−110] but such calculations are extremely challenging and will not be discussed further. Because the electronic coupling is a prefactor in the rate constant expression, relative rate constants for molecules expected to have similar electronic couplings can be calculated without knowledge of this parameter. In many cases, obtaining the relative rate constants for a series of related molecules is sufficient for catalyst design.

C. EPT Reactions. We have developed a general theoretical formulation for PCET reactions. Because of space limitations, we summarize this theory here and refer the reader to other reviews for more details.[6,7,22] The simplest PCET reaction, which involves the transfer of one electron and one proton, can be represented by the four states shown in Scheme 4. The

Scheme 4. PCET Sequential (PT−ET and ET−PT) and Concerted (EPT) Mechanisms

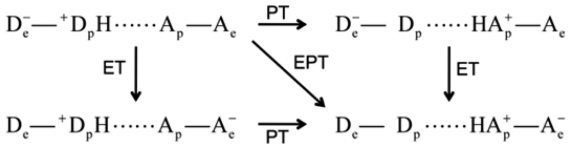

sequential mechanisms correspond to following along the outside edges of the rectangle: either PT followed by ET or ET followed by PT. The concerted mechanism, denoted EPT, corresponds to following the diagonal. The mechanism is determined by the relative energies and couplings among these four states. When the off-diagonal states are much higher in energy, the reaction tends to be concerted, following the diagonal, to avoid the high-energy intermediates.

The EPT mechanism can be depicted in terms of free energy curves along a collective solvent coordinate, as depicted in Figure 4. The blue curve corresponds to the reactant, in which the electron is localized on the donor, and the red curve corresponds to the product, in which the electron is localized on the acceptor. In this theory, the transferring hydrogen nucleus and all electrons are treated quantum mechanically. Thus, these free energy curves correspond to mixed electron−proton vibronic states. Figure 4 shows only the lowest-energy

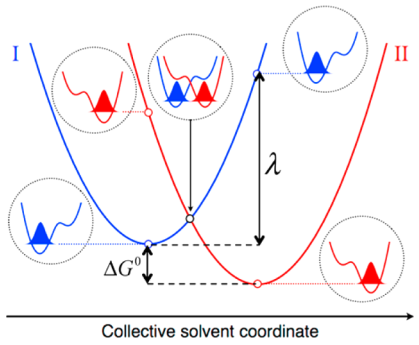

Figure 4. Free energy curves for the ground reactant (I) and product (II) diabatic electron−proton vibronic states along the collective solvent coordinate for an EPT reaction. The reactant (blue) and product (red) diabatic states correspond to the electron localized on the donor and acceptor, respectively. The proton potential energy curves along the proton coordinate and the corresponding ground state proton vibrational wave functions are depicted for the reactant minimum, the crossing point, and the product minimum of the free energy curves. The energies of these proton vibrational states correspond to the open circles on the free energy curves. The proton potential energy curves associated with the crossing point are shifted higher in energy for clarity. The figure and caption were reproduced with permission from ref 6. Copyright 2008 American Chemical Society.

reactant and product vibronic states. There are actually two sets of nested parabolas corresponding to the different proton vibrational states for each electronic state. Figure 4 also depicts the proton potential energy curves for specific values of the collective solvent coordinate. For the reactant (blue curves), the proton donor well is lower in energy, whereas for the product (red curves), the proton acceptor well is lower in energy. At the crossing point of the free energy curves, the ground reactant and product proton vibrational states are degenerate. The overlap between the proton vibrational wave functions at this point, depicted in Figure 5, strongly influences the rate constants and kinetic isotope effects.

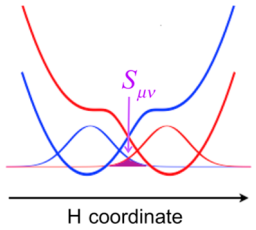

Figure 5. Reactant (blue) and product (red) proton potential energy curves along the proton coordinate and the corresponding ground state proton vibrational wave functions, with the overlap $S_{\mu\nu}$ shown in purple.

The simplest nonadiabatic rate constant for EPT reactions is[6,111]

$$k^{\mathrm{EPT}} = \sum_{\mu} P_{\mu} \sum_{\nu} \frac{|V^{\mathrm{el}} S_{\mu\nu}|^2}{\hbar} \sqrt{\frac{\pi}{\lambda k_{\mathrm{B}} T}} \exp\left[-\frac{(\Delta G^{\circ}_{\mu\nu} + \lambda)^2}{4\lambda k_{\mathrm{B}} T}\right] \quad (19)$$

where the summations are over reactant and product vibronic states, P_{μ} is the Boltzmann probability for the reactant state μ, V^{el} is the electronic coupling, $S_{\mu\nu}$ is the overlap between the reactant and product proton vibrational wave functions for

dx.doi.org/10.1021/ic5002896 | Inorg. Chem. 2014, 53, 6427−6443

states μ and ν, λ is the reorganization energy, and $\Delta G^{\circ}_{\mu\nu}$ is the reaction free energy for states μ and ν. The reorganization energy and reaction free energy are depicted in Figure 4, and the overlap is depicted in Figure 5.

The proton donor−acceptor distance strongly impacts the overlap between the reactant and product proton vibrational wave functions: the larger the proton donor−acceptor distance, the smaller the overlap. Thus, we have extended this theory to include the effects of the proton donor−acceptor motion.[6,112] We have also extended this theory to electrochemical EPT.[113] In this case, we assume that a PT reaction occurs within a solvated molecular complex, corresponding to either intramolecular PT within a single molecule or intermolecular PT within a hydrogen-bonded adduct. In the electrochemical EPT reaction, the electron transfers between the molecular complex and the electrode, while the proton transfers within the molecular complex. The general theoretical concepts discussed above for homogeneous EPT are also valid for electrochemical EPT, but the acceptor state is now a continuum of electronic states associated with the conduction band of the electrode.

We have derived rate constant expressions for electrochemical EPT in various well-defined regimes.[113,114] The anodic and cathodic nonadiabatic EPT rate constants are

$$k_a^{EPT}(\eta; R) = \sum_{\mu,\nu} P_\mu \frac{(V^{el}S_{\mu\nu})^2}{\beta'\hbar}\sqrt{\frac{\pi}{k_B T\lambda}}\rho_M \int d\varepsilon\,[1 - f(\varepsilon)] \exp\left[-\frac{(\Delta\tilde{U}_{\mu\nu} + \varepsilon - e\eta + \lambda)^2}{4\lambda k_B T}\right]$$

$$k_c^{EPT}(\eta; R) = \sum_{\mu,\nu} P_\nu \frac{(V^{el}S_{\mu\nu})^2}{\beta'\hbar}\sqrt{\frac{\pi}{k_B T\lambda}}\rho_M \int d\varepsilon\, f(\varepsilon) \exp\left[-\frac{(-\Delta\tilde{U}_{\mu\nu} - \varepsilon + e\eta + \lambda)^2}{4\lambda k_B T}\right] \quad (20)$$

where the summations are over proton vibrational states μ of the reduced solute complex and ν of the oxidized solute complex and R is the fixed proton donor−acceptor distance. The quantity $\Delta\tilde{U}_{\mu\nu}$ is defined as $\Delta\tilde{U}_{\mu\nu} = \Delta U_{\mu\nu} + k_B T \ln(Q^{II}/Q^{I})$, where $\Delta U_{\mu\nu}$ is the energy difference between states ν and μ and Q^{I} and Q^{II} are the vibrational partition functions of the reduced and oxidized solute complexes, respectively, in bulk solution. The other quantities are defined in the same way as in homogeneous EPT. The quantities P_μ, $S_{\mu\nu}$, and $\Delta\tilde{U}_{\mu\nu}$ depend on the proton donor−acceptor distance R.

The effects of the proton donor−acceptor motion can be included in several different ways. We have derived analytical EPT rate constant expressions that include these effects in certain well-defined regimes.[113,114] An alternative approach that is often more suitable for electrochemical EPT is to thermally average the rate constant over the proton donor−acceptor distance.[115] The resulting anodic and cathodic rate constants are given as

$$k_a^{EPT}(\eta) = \int P_a(R)\, k_a^{EPT}(\eta; R)\, dR$$

$$k_c^{EPT}(\eta) = \int P_c(R)\, k_c^{EPT}(\eta; R)\, dR \quad (21)$$

where $P_a(R)$ and $P_c(R)$ are the probability distribution functions for the anodic and cathodic processes, respectively. (In certain implementations, the reference for the overpotential must be shifted by a constant.[115,116]) In these expressions, the rate constant for each distance R is weighted by the probability of sampling that distance R. Often these probability distribution functions are chosen to correspond to a classical harmonic oscillator and depend on an effective force constant k_{eff} and equilibrium proton donor−acceptor distance $\bar{R}$. For large force constants associated with high-frequency vibrations of the proton donor−acceptor mode, a quantum mechanical harmonic oscillator probability distribution function is more appropriate.[117] Alternatively, anharmonic probability distribution functions could be obtained from electronic structure calculations or molecular dynamics simulations.

D. Microkinetic Modeling. After calculation of the rate constants for the PT, ET, and EPT reactions among the various species, the system can be studied with microkinetic modeling.[26−28] In microkinetic analysis, all elementary steps in the reaction mechanism are considered explicitly without any assumptions about the rate-determining step. The various reactions are then combined in a set of coupled equations that rely on the rate constants, and the system of equations is solved numerically. This approach is likely to become a powerful tool in catalyst design but will not be discussed further here.

VII. NICKEL-BASED CATALYSTS WITH PENDANT AMINES

A promising class of electrocatalysts for H_2 oxidation and production is the nickel-based catalysts with pendant amines depicted in Chart 3.[118−121] In these $Ni(P_2N_2)_2$ catalysts (P_2N_2 = 1,5-diaza-3,7-diphosphacyclooctane), the pendant amine is positioned over the metal center to assist in the shuttling of protons to and from the metal center and possibly to facilitate the coupling between ET and PT reactions. These catalysts, as well as other related catalysts,[122−127] were modeled after hydrogenase enzymes, which are thought to utilize an amine group near the metal center for this purpose.[128−132] Depending on the substituents on the phosphorus and nitrogen atoms, as well as the experimental conditions, these catalysts can catalyze H_2 oxidation or production. These complexes have been shown to produce H_2 at turnover frequencies as large as 10^3−10^5 s^{-1} with moderate overpotentials.[133−136] Figure 6 depicts a proposed catalytic cycle, where H_2 production corresponds to the counterclockwise direction. We emphasize that this catalytic cycle does not pertain to all $Ni(P_2N_2)_2$ catalysts. In particular, the specific order of the various ET and PT steps depends on the substituents and on the experimental conditions, such as the strength and concentration of acid. Moreover, pathways involving chair-to-boat isomerizations of the rings, as well as additional doubly protonated states, have also been observed.

Chart 3. $Ni(P_2N_2)_2$ Catalysts

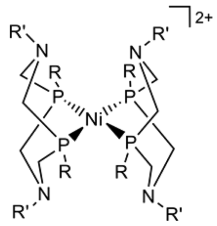

dx.doi.org/10.1021/ic5002896 | Inorg. Chem. 2014, 53, 6427−6443

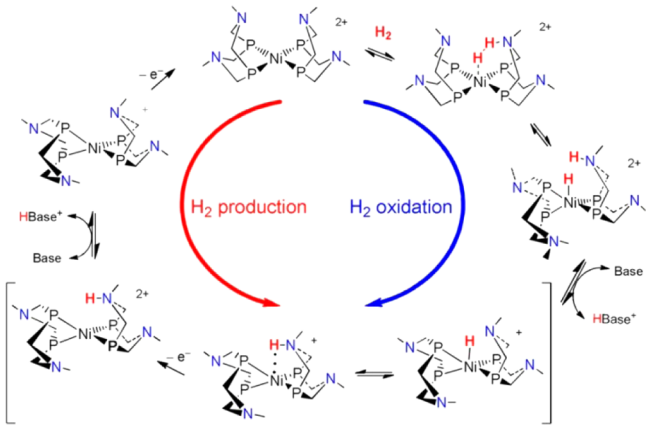

Figure 6. Proposed mechanism of H_2 oxidation (blue path) and production (red path) for the $[Ni(P_2N_2)_2]^{2+}$ electrocatalyst. Ligands bound to phosphorus and nitorgen atoms are omitted for clarity. The square brackets indicate the PCET reaction that has been studied with nonadiabatic EPT theory. The figure was reproduced with permission from ref 17. Copyright 2012 American Chemical Society.

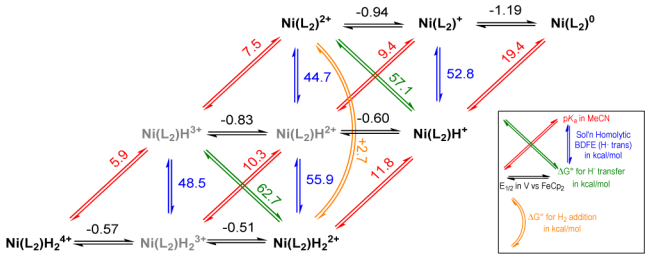

Figure 7. Experimental and calculated thermodynamic data for the $Ni(P_2N_2)_2$ catalyst (L = P_2N_2) with phenyl groups bound to the phosphorus atoms and benzyl groups bound to the nitrogen atoms (Chart 3; R = phenyl and R′ = benzyl). The thermodynamic scheme shows the relationships among the species in terms of $E_{1/2}$, pK_a, homolytic solution bond dissociation free energy (BDFE), $\Delta G^\circ_{H^-}$, and $\Delta G^\circ_{H_2}$ values. Formulas are intended to indicate only composition and not structure (i.e., the notation does not distinguish between nickel hydrides and protonated pendant amines). The species in gray have not been directly observed experimentally, and their relative stabilities were therefore determined from theoretical calculations. A version of this scheme was reported in ref 138, but this specific figure was reproduced with permission from ref 32. Copyright 2013 American Chemical Society.

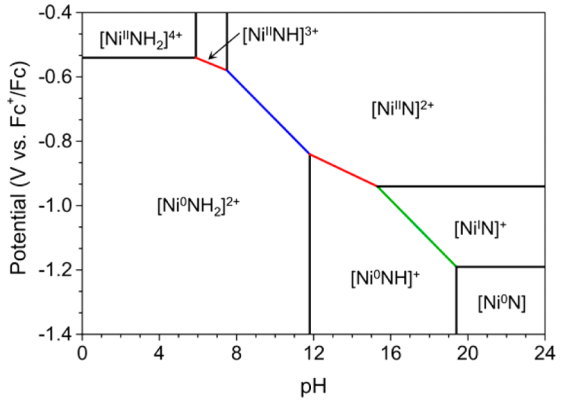

Figure 8. Pourbaix diagram for the $Ni(P_2N_2)_2$ catalyst shown in Chart 3 with R = phenyl and R′ = benzyl. The horizontal and vertical lines are the reduction potentials and pK_a's, respectively, of various protonated and unprotonated forms of the catalyst. The red lines have negative slopes of ~29.5 mV/pH unit and correspond to $2e^- - 1H^+$ processes. The blue line has a negative slope of ~59 mV/pH unit and corresponds to a $2e^- - 2H^+$ process. The green line has a negative slope of ~59 mV/pH unit and corresponds to a $1e^- - 1H^+$ process. Because this diagram represents the electrocatalyst in acetonitrile, the *x*-axis label of pH implicitly denotes the pK_a of the acid in acetonitrile, and the Pourbaix diagram depicts the most thermodynamically stable species for a given reduction potential and acid strength. The figure was reproduced with permission from ref 32. Copyright 2013 American Chemical Society.

The $Ni(P_2N_2)_2$ systems have been studied extensively with theoretical methods. When appropriate methods and references are used, the calculated reduction potentials and pK_a's agree well with the available experimental data.[15,17] Moreover, linear free energy correlations analogous to those shown in Figure 2 for the cobaloximes have also been identified for these types of catalysts.[137] Instead of the Hammett constants, the thermodynamic properties were linearly correlated with each other for a series of substituents on the nitrogen and phosphorus atoms. These analyses revealed that all of the thermodynamic properties, including the reduction potentials and the pK_a values associated with the nickel center and the pendant amine, can be estimated on the basis of the unprotonated $Ni^{II/I}$ and $Ni^{I/0}$ reduction potentials and the pK_a of the parent primary aminium ion.[137] Within this framework, experimental measurements or calculations of these three properties enable the generation of the complete thermodynamic scheme for these catalysts.

Even without using these types of linear correlations, the complete thermodynamic scheme and Pourbaix diagram can be generated for a given catalyst using a combination of experimental and theoretical data. As an example, consider the $Ni(P_2N_2)_2$ system shown in Chart 3 with R = phenyl and R′ = benzyl.[32] The reduction potentials and pK_a's for the various species involved in catalysis have been measured experimentally and/or calculated theoretically. The resulting thermodynamic scheme is depicted in Figure 7.[32] We emphasize that this scheme is the result of a combination of experimental and theoretical data and would be incomplete without this synergy. Moreover, this scheme has mechanistic implications in that it allows the generation of thermodynamic reaction pathways for the various possible mechanisms, analogous to Figure 1 for the cobaloximes. In this manner, the thermodynamically favorable reaction pathways can be identified.

In addition, these thermodynamic data enable construction of the Pourbaix diagram shown in Figure 8.[32] As discussed in section III, the Pourbaix diagram indicates the most thermodynamically stable species at each reduction potential and pH value. For nonaqueous solvents, such as acetonitrile, the Pourbaix diagram depicts the most thermodynamically stable species for a given reduction potential and acid strength, and the *x*-axis label of pH implicitly denotes the pK_a of the acid in the specified solvent. The horizontal and vertical black lines correspond to the reduction potentials and pK_a's, respectively, of the various species indicated on the diagram. The diagonal lines correspond to coupled electron-proton transfer processes, and the slopes indicate the number of electrons and protons transferred, according to the Nernst equation associated with eq 14. The blue and green lines have negative slopes of ~59 mV/pH unit, indicating that the same number of electrons and protons are transferred. Specifically, the blue line corresponds to a $2e^- - 2H^+$ process, and the green line corresponds to a

dx.doi.org/10.1021/ic5002896 | Inorg. Chem. 2014, 53, 6427−6443

$1e^--1H^+$ process. The red lines have negative slopes of ~29.5 mV/pH unit and correspond to $2e^--1H^+$ processes.

On the basis of this Pourbaix diagram, we can deduce that the mechanism for this catalyst differs from that shown in Figure 6 when strong acids are used. Specifically, the catalyst is expected to be doubly protonated prior to the initial reduction step in the presence of very strong acids, suggesting a PT–PT–ET–ET mechanism under these conditions. This result is consistent with experimental cyclic voltammetry measurements of the pH dependence of the reduction potentials for these catalysts.[32,138] The Nernstian response observed experimentally corresponds to moving down the blue diagonal line in Figure 8 as the pK_a of the acid is increased. Note that the details of the Pourbaix diagram will depend on the experimental data used, as well as the level of theory and underlying assumptions, such as the presence of axial solvent ligands.[32,137]

So far we have discussed only the thermodynamic aspects of the $Ni(P_2N_2)_2$ catalysts. As discussed in section VI, however, the mechanism depends on kinetic as well as thermodynamic considerations. The free energy barriers for certain chair-to-boat isomerization and PT steps have been calculated for these molecular electrocatalysts with DFT.[17,139] These free energy barriers can be used to estimate the rate constants for these steps using transition state theory, as in eq 15. In addition, the inner-sphere and solvent reorganization energies have been calculated for some of the $Ni(P_2N_2)_2$ catalysts.[17,116] These reorganization energies can be used to estimate the rate constants for ET steps using Marcus theory, as in eq 16. Thus, the kinetics of the individual ET and PT steps has been probed.

The calculation of rate constants for the concerted mechanism, EPT, is more challenging but has been performed for the $Ni(P_2N_2)_2$ catalyst shown in Chart 3 with R = R′ = CH_3.[116] The portion of the catalytic cycle that was studied with the PCET theory described in section VI.C is indicated by square brackets in Figure 6. In these steps, an electron is transferred between the complex and the electrode, and a proton is transferred between the pendant amine nitrogen and the nickel center. Thus, the proton donor–acceptor distance R is the distance between the nickel and nitrogen atoms, and we designated a one-dimensional axis along which the hydrogen moves as it transfers. We performed geometry optimizations for a series of constrained Ni–N distances and generated proton potentials along the one-dimensional hydrogen coordinate for the reduced and oxidized states. The proton potentials are asymmetric double wells, as depicted schematically in Figure 5, with the well near the nickel atom lower in energy for the reduced state (i.e., blue potential curve in Figure 5) and the well near the nitrogen atom lower in energy for the oxidized state (i.e., red potential curve). For smaller Ni–N distances, the overlap between the proton vibrational wave functions (depicted in purple in Figure 5 for the ground states) is larger, leading to a higher rate constant.

The details of the EPT rate constant calculations are described in ref 116, and here we provide only a brief summary. First, the rate constants for the series of Ni–N distances were calculated using eq 20 to obtain the anodic and cathodic rate constants, $k_a(R)$ and $k_c(R)$, which increase dramatically as R decreases because of the overlap factor mentioned above. Then, the probability distribution functions, $P_a(R)$ and $P_c(R)$, for the Ni–N motion were determined from the equilibrium Ni–N distance and the effective frequency associated with this vibrational motion. These probability distribution functions reflect the probability of sampling each

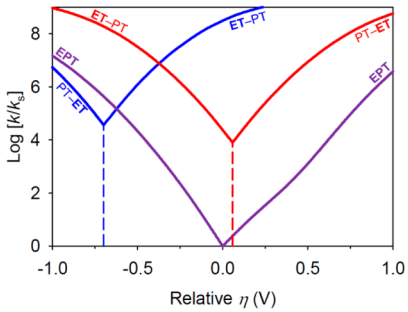

Figure 9. Calculated electrochemical rate constants as functions of the potential for the ET and EPT reactions that could occur for the $Ni(P_2N_2)_2$ catalysts shown in Chart 3 (R = R′ = CH_3). The rate constants are given relative to k_s, the standard rate constant for the EPT reaction. The standard potential for the EPT reaction is chosen to be zero overpotential ($\eta = 0$), and the standard potentials for the ET reactions are shifted relative to this value by their relative reduction potentials. Thus, the overpotential η is defined to be the applied potential relative to the standard potential for the EPT reaction. The blue curve is associated with ET for the complex with the proton on the nickel center, and the red curve is associated with ET for the complex with the proton on the nitrogen of the pendant amine. The purple curve is associated with the EPT process that involves both ET and intramolecular PT between the nickel center and the nitrogen of the pendant amine. Note that these plots are not experimentally accessible for this electrocatalyst because of complications due to other steps in the catalytic cycle. The figure was adapted from ref 116.

Ni–N distance. Finally, the total rate constant was calculated using eq 21, where the rate constant for each distance R is weighted by the probability of sampling that distance. Figure 9 depicts the calculated Tafel plots, which show the ET and EPT rate constants as functions of the overpotential, for the $Ni(P_2N_2)_2$ catalyst shown in Chart 3 with R = R′ = CH_3. These calculated Tafel plots indicate that the dominant mechanism (i.e., ET–PT, PT–ET, or EPT) depends on the overpotential.[116] Thus, again the experimental conditions can be used to alter the mechanism. Note that these Tafel plots are not experimentally accessible for this electrocatalyst because of complications due to other steps in the catalytic cycle.

An important prediction arising from the EPT rate constant calculations is that the EPT mechanism will be favored by decreasing the equilibrium Ni–N distance and the effective frequency associated with this mode.[116] The smaller equilibrium Ni–N distance will favor shorter distances with larger overlap factors, thereby increasing the rate constant. The lower effective frequency for the Ni–N motion will allow the system to sample smaller Ni–N distances with a lower energetic penalty, thereby enhancing the total rate constant. Thus, these studies suggested that flexible ligands may be more effective for a concerted mechanism because of the lower energetic penalty associated with the nitrogen moving toward the nickel to facilitate PT.

On the basis of this theoretical prediction, we investigated several complexes with more flexible ligands.[140] However, we found that the equilibrium Ni–N distance tends to be larger when the ligand is more flexible, thereby counteracting the advantages of the lower frequency of the Ni–N motion. We also found that steric clashes could be eliminated by replacing bulky substituents with smaller substituents to decrease the energetic penalty of the nitrogen moving toward the nickel. Overall, this study illustrated that a combination of eliminating the steric clashes and obtaining a balance between ligand

dx.doi.org/10.1021/ic5002896 | Inorg. Chem. 2014, 53, 6427–6443

flexibility and sufficient positioning of the pendant amine will favor the concerted mechanism.[140]

This section has highlighted the usefulness of theoretical calculations for understanding the mechanisms, thermodynamics, and kinetics of molecular electrocatalysts and for guiding the design of such catalysts. The predictive power provided by the free energy linear correlations can help to tune the thermodynamic properties of the catalysts. The predictions of rate constants for PT, ET, and EPT may help to optimize the rate constants. Moreover, the prediction that flexible ligands may favor the concerted mechanism could be helpful in the design of catalysts with lower overpotentials because the concerted mechanism is expected to require a lower overpotential by avoiding high-energy intermediates. Nevertheless, these catalysts are still not completely understood. The overall catalytic cycle involves many ET and PT steps, which could occur either sequentially or concertedly, as well as various chair-to-boat isomerization steps. While focusing on individual steps is useful, the complete catalytic cycle must be considered in its entirety for catalyst design. Using the various rate constants described in this section, microkinetic modeling could be performed to examine the overall catalytic cycle and provide a more global understanding of these catalysts.

VIII. OVERVIEW OF CATALYST DESIGN

The ultimate goal of catalyst design is to maximize the turnover frequency and minimize the overpotential. As illustrated by the examples given above, the catalytic cycles for molecular electrocatalysts are often complicated, involving many steps that could occur either sequentially or concertedly, following a variety of sequences. To develop renewable energy sources, the catalysts should be comprised of environmentally friendly, cost-effective, and earth-abundant materials. These restrictions place even greater challenges on catalyst design. Nevertheless, progress has been made in the development of computational methods for investigating both the thermodynamics and kinetics of these catalytic cycles and thereby guiding the design of more effective catalysts.

Several different strategies can be used in the design of more effective molecular electrocatalysts. Many of the existing strategies focus on thermodynamic aspects. The reduction potentials and pK_a's can be tuned by altering the substituents on the ligands to be either more or less electron-withdrawing or electron-donating. Linear free energy correlations among these properties can be used to make predictions about the impact of the substituents on the reduction potentials and pK_a's and to determine all of these properties from one or a few of them.[18] This strategy was successful with the cobaloximes[65] and the $Ni(P_2N_2)_2$ catalysts.[15] In addition, the ligands themselves can be modified, such as the replacement of O−BF_2−O bridges with O−H−O bridges in the cobaloximes.[80] Moreover, upon modification of the ligands, the role of noninnocent ligands, namely, ligand protonation or reduction, can be utilized advantageously. For example, ligands that are more easily protonated may decrease the required overpotential, as observed for the cobalt dithiolenes[69] and the cobaloximes with the O−H−O bridge.[80]

In some cases, ligand modification and substituent effects can change the mechanism as well as the thermodynamics. For example, calculations and cyclic voltammetry experiments suggest that the cobaloxime with methyl substituents may favor a monometallic pathway, while the cobaloxime with phenyl substituents may favor a bimetallic pathway, under certain experimental conditions.[16,65,73,74,77] Moreover, certain substituents on the ligands cause $Ni(P_2N_2)_2$ to follow a PT−PT−ET−ET mechanism in the presence of very strong acids, while other $Ni(P_2N_2)_2$ electrocatalysts follow a mechanism that starts with an initial reduction step prior to protonation.[32] In addition, ligands that are more easily reduced can change the mechanism by accepting the electron instead of the metal center. Finally, modifying the metals themselves can lead to different thermodynamic properties and mechanisms.

The thermodynamic and kinetic information obtained from theoretical calculations can be used to generate thermodynamic schemes, reaction pathways, Pourbaix diagrams, and Tafel plots or rate diagrams. In turn, this information can be used to identify the thermodynamically and kinetically favorable mechanisms under specified experimental conditions. These types of diagrams clearly illustrate the dependence of the mechanism and rate on experimental conditions such as the acid strength and concentration, as well as the overpotential. Examples of the impact of experimental conditions were given above in the context of both the cobaloximes[16,65] and $Ni(P_2N_2)_2$ catalysts.[15,32,116]

Additional aspects of catalyst design can be revealed by examining both sequential and concerted PCET mechanisms. The concerted mechanism is thought to be advantageous in terms of decreasing the overpotential. Thus, catalysts can be designed to favor the concerted PCET mechanism. For the $Ni(P_2N_2)_2$ catalysts, theoretical calculations suggested that the concerted mechanism will be favored by designing more flexible ligands that also maintain a short equilibrium proton donor−acceptor distance.[116,140] However, finding this balance between ligand flexibility and a well-positioned pendant amine is challenging.

Overall, theoretical methods have been shown to assist in interpreting experimental data and guiding the design of more effective molecular electrocatalysts. However, investigating individual steps in the catalytic cycle may be misleading because these steps may not be determining the turnover frequency or the overpotential. To obtain a more global picture, microkinetic modeling can be used to describe all possible mechanisms simultaneously and to determine which types of modifications would lead to an overall higher turnover frequency and lower overpotential. In addition, theoretical calculations should be combined with experimental studies, ensuring continual feedback between theory and experiment, to optimize progress in catalyst design.

AUTHOR INFORMATION

Corresponding Author

*E-mail: shs3@illinois.edu.

Notes

The authors declare no competing financial interest.

ACKNOWLEDGMENTS

We are very grateful to Soumya Ghosh, Alexander Soudackov, Mioy Huynh, and Samantha Horvath for useful discussions and helpful advice. The research on the metal oximes and cobalt dithiolenes was supported by the NSF under Grant CHE-1305124. The research on the $Ni(P_2N_2)_2$ catalysts was supported as part of the Center for Molecular Electrocatalysis, an Energy Frontier Research Center funded by the U.S. Department of Energy, Office of Science, Office of Basic Energy Sciences.

REFERENCES

(1) Wilson, A. D.; Shoemaker, R. K.; Miedaner, A.; Muckerman, J. T.; DuBois, D. L.; DuBois, M. R. *Proc. Natl. Acad. Sci. U.S.A.* **2007**, *104*, 6951−6956.
(2) Marinescu, S. C.; Winkler, J. R.; Gray, H. B. *Proc. Natl. Acad. Sci. U.S.A.* **2012**, *109*, 15127−15131.
(3) Cukier, R. I.; Nocera, D. G. *Annu. Rev. Phys. Chem.* **1998**, *49*, 337−369.
(4) Mayer, J. M. *Annu. Rev. Phys. Chem.* **2004**, *55*, 363−390.
(5) Huynh, M. H. V.; Meyer, T. J. *Chem. Rev.* **2007**, *107*, 5004−5064.
(6) Hammes-Schiffer, S.; Soudackov, A. V. *J. Phys. Chem. B* **2008**, *112*, 14108−14123.
(7) Hammes-Schiffer, S.; Stuchebrukhov, A. A. *Chem. Rev.* **2010**, *110*, 6939−6960.
(8) Hammes-Schiffer, S. *Energy Environ. Sci.* **2012**, *5*, 7696−7703.
(9) Nørskov, J. K.; Rossmeisl, J.; Logadottir, A.; Lindqvist, L.; Kitchin, J. R.; Bligaard, T.; Jónsson, H. *J. Phys. Chem. B* **2004**, *108*, 17886−17892.
(10) Baik, M.-H.; Friesner, R. A. *J. Phys. Chem. A* **2002**, *106*, 7407−7412.
(11) Roy, L. E.; Jakubikova, E.; Guthrie, M. G.; Batista, E. R. *J. Phys. Chem. A* **2009**, *113*, 6745−6750.
(12) Tsai, M.-K.; Rochford, J.; Polyansky, D. E.; Wada, T.; Tanaka, K.; Fujita, E.; Muckerman, J. T. *Inorg. Chem.* **2009**, *48*, 4372−4383.
(13) Wang, T.; Brudvig, G. W.; Batista, V. S. *J. Chem. Theory Comput.* **2010**, *6*, 755−760.
(14) Wang, T.; Brudvig, G. W.; Batista, V. S. *J. Chem. Theory Comput.* **2010**, *6*, 2395−2401.
(15) Chen, S.; Rousseau, R.; Raugei, S.; Dupuis, M.; DuBois, D. L.; Bullock, R. M. *Organometallics* **2011**, *30*, 6108−6118.
(16) Solis, B. H.; Hammes-Schiffer, S. *Inorg. Chem.* **2011**, *50*, 11252−11262.
(17) Fernandez, L. E.; Horvath, S.; Hammes-Schiffer, S. *J. Phys. Chem. C* **2012**, *116*, 3171−3180.
(18) Araujo, C. M.; Doherty, M. D.; Konezny, S. J.; Luca, O. R.; Usyatinsky, A.; Grade, H.; Lobkovsky, E.; Soloveichik, G. L.; Crabtree, R. H.; Batista, V. S. *Dalton Trans.* **2012**, *41*, 3562−3573.
(19) Sundstrom, E. J.; Yang, X.; Thoi, V. S.; Karunadasa, H. I.; Chang, C. J.; Long, J. R.; Head-Gordon, M. *J. Am. Chem. Soc.* **2012**, *134*, 5233−5242.
(20) Keith, J. A.; Grice, K. A.; Kubiak, C. P.; Carter, E. A. *J. Am. Chem. Soc.* **2013**, *135*, 15823−15829.
(21) Borgis, D.; Hynes, J. T. *Chem. Phys.* **1993**, *170*, 315−346.
(22) Layfield, J. P.; Hammes-Schiffer, S. *Chem. Rev.* **2014**, DOI: 10.1021/cr400400p.
(23) Marcus, R. A.; Sutin, N. *Biochim. Biophys. Acta* **1985**, *811*, 265−322.
(24) Cukier, R. I. *J. Phys. Chem.* **1996**, *100*, 15428−15443.
(25) Hammes-Schiffer, S. *Acc. Chem. Res.* **2009**, *42*, 1881−1889.
(26) Dumesic, J. A.; Rudd, D. F.; Aparicio, L. M.; Rekoske, J. E.; Treviño, A. A. *The Microkinetics of Heterogeneous Catalysis*; American Chemical Society: Washington, DC, 1993.
(27) Broadbelt, L. J.; Snurr, R. Q. *Appl. Catal. A:Gen* **2000**, *200*, 23−46.
(28) Kozuch, S.; Shaik, S. *Acc. Chem. Res.* **2011**, *44*, 101−110.
(29) Muckerman, J. T.; Fujita, E. *Chem. Commun.* **2011**, *47*, 12456−12458.
(30) Konezny, S. J.; Doherty, M. D.; Luca, O. R.; Crabtree, R. H.; Soloveichik, G. L.; Batista, V. S. *J. Phys. Chem. C* **2012**, *116*, 6349−6356.
(31) Ribeiro, R. F.; Marenich, A. V.; Cramer, C. J.; Truhlar, D. G. *J. Phys. Chem. B* **2011**, *115*, 14556−14562.
(32) Horvath, S.; Fernandez, L. E.; Appel, A. M.; Hammes-Schiffer, S. *Inorg. Chem.* **2013**, *52*, 3643−3652.
(33) Bartmess, J. E. *J. Phys. Chem.* **1994**, *98*, 6420−6424.
(34) Lewis, A.; Bumpus, J. A.; Truhlar, D. G.; Cramer, C. J. *J. Chem. Educ.* **2004**, *81*, 596.
(35) Isse, A. A.; Gennaro, A. *J. Phys. Chem. B* **2010**, *114*, 7894−7899.
(36) Lim, C.; Bashford, D.; Karplus, M. *J. Phys. Chem.* **1991**, *95*, 5610−5620.
(37) Schüürmann, G.; Cossi, M.; Barone, V.; Tomasi, J. *J. Phys. Chem. A* **1998**, *102*, 6706−6712.
(38) Tissandier, M. D.; Cowen, K. A.; Feng, W. Y.; Gundlach, E.; Cohen, M. H.; Earhart, A. D.; Coe, J. V.; Thomas, R.; Tuttle, J. *J. Phys. Chem. A* **1998**, *102*, 7787−7794.
(39) Hwang, S.; Chung, D. S. *Bull. Korean Chem. Soc.* **2005**, *26*, 589−593.
(40) Grabowski, P.; Riccardi, D.; Gomez, M. A.; Asthagiri, D.; Pratt, L. R. *J. Phys. Chem. A* **2002**, *106*, 9145−9148.
(41) Kelly, C. P.; Cramer, C. J.; Truhlar, D. G. *J. Phys. Chem. B* **2007**, *111*, 408−422.
(42) Reiss, H.; Heller, A. *J. Phys. Chem.* **1985**, *89*, 4207−4213.
(43) Trasatti, S. *Pure Appl. Chem.* **1986**, *58*, 955−966.
(44) Fawcett, W. R. *Langmuir* **2008**, *24*, 9868−9875.
(45) Qi, X.-J.; Fu, Y.; Liu, L.; Guo, Q.-X. *Organometallics* **2007**, *26*, 4197−4203.
(46) Fourmond, V.; Jacques, P.-A.; Fontecave, M.; Artero, V. *Inorg. Chem.* **2010**, *49*, 10338−10347.
(47) Ciancanelli, R.; Noll, B. C.; DuBois, D. L.; DuBois, M. R. *J. Am. Chem. Soc.* **2002**, *124*, 2984−2992.
(48) van Duijneveldt, F. B.; van Duijneveldt-van de Rijdt, J. G. C. M.; van Lenthe, J. H. *Chem. Rev.* **1994**, *94*, 1873−1885.
(49) Kohn, W.; Sham, L. J. *Phys. Rev.* **1965**, *140*, A1133−A1138.
(50) Parr, R. G.; Yang, W. *Density-Functional Theory of Atoms and Molecules*; Oxford University Press: Oxford, U.K.,, 1989.
(51) Chen, S.; Raugei, S.; Rousseau, R.; Dupuis, M.; Bullock, R. M. *J. Phys. Chem. A* **2010**, *114*, 12716−12724.
(52) Minenkov, Y.; Singstad, Å.; Occhipinti, G.; Jensen, V. R. *Dalton Trans.* **2012**, *41*, 5526−5541.
(53) Ditchfield, R.; Hehre, W. J.; Pople, J. A. *J. Chem. Phys.* **1971**, *54*, 724−728.
(54) Hehre, W. J.; Ditchfield, R.; Pople, J. A. *J. Chem. Phys.* **1972**, *56*, 2257−2261.
(55) Francl, M. M.; Pietro, W. J.; Hehre, W. J.; Binkley, J. S.; Gordon, M. S.; DeFrees, D. J.; Pople, J. A. *J. Chem. Phys.* **1982**, *77*, 3654−3665.
(56) Frenking, G.; Antes, I.; Böhme, M.; Dapprich, S.; Ehlers, A. W.; Jonas, V.; Neuhaus, A.; Otto, M.; Stegmann, R.; Veldkamp, A.; Vyboishchikov, S. F. Pseudopotential Calculations of Transition Metal Compounds: Scope and Limitations. In *Reviews in Computational Chemistry*; Lipkowitz, K. B., Boyd, D. B., Eds.; VCH Publishers, Inc.: New York, 1996; Vol. *8*.
(57) Miertuš, S.; Scrocco, E.; Tomasi, J. *Chem. Phys.* **1981**, *55*, 117−129.
(58) Miertuš, S.; Tomasi, J. *Chem. Phys.* **1982**, *65*, 239−245.
(59) Barone, V.; Cossi, M. *J. Phys. Chem. A* **1998**, *102*, 1995−2001.
(60) Cossi, M.; Rega, N.; Scalmani, G.; Barone, V. *J. Comput. Chem.* **2003**, *24*, 669−681.
(61) Warshel, A.; Parson, W. W. *Annu. Rev. Phys. Chem.* **1991**, *42*, 279−309.
(62) Van Voorhis, T.; Kowalczyk, T.; Kaduk, B.; Wang, L.-P.; Cheng, C.-L.; Wu, Q. *Annu. Rev. Phys. Chem.* **2010**, *61*, 149−170.
(63) Hughes, T. F.; Friesner, R. A. *J. Phys. Chem. B* **2011**, *115*, 9280−9289.
(64) Pourbaix, M. *Atlas of Electrochemical Equilibria in Aqueous Solutions*, 2nd ed.; NACE International: Houston, TX, 1974.
(65) Solis, B. H.; Hammes-Schiffer, S. *J. Am. Chem. Soc.* **2011**, *133*, 19036−19039.
(66) Hansch, C.; Leo, A.; Taft, R. W. *Chem. Rev.* **1991**, *91*, 165−195.
(67) McNamara, W. R.; Han, Z.; Alberin, P. J.; Brennessel, W. W.; Holland, P. L.; Eisenberg, R. *J. Am. Chem. Soc.* **2011**, *133*, 15368−15371.
(68) McNamara, W. R.; Han, Z.; Yin, C.-J.; Brennessel, W. W.; Holland, P. L.; Eisenberg, R. *Proc. Natl. Acad. Sci. U.S.A.* **2012**, *109*, 15594−15599.
(69) Solis, B. H.; Hammes-Schiffer, S. *J. Am. Chem. Soc.* **2012**, *134*, 15253−15256.
(70) Chirik, P. J. *Inorg. Chem.* **2011**, *50*, 9737−9740.

(71) Kaim, W. *Inorg. Chem.* **2011**, *50*, 9752−9765.
(72) Eisenberg, R.; Gray, H. B. *Inorg. Chem.* **2011**, *50*, 9741−9751.
(73) Hu, X.; Cossairt, B. M.; Brunschwig, B. S.; Lewis, N. S.; Peters, J. C. *Chem. Commun.* **2005**, 4723−4725.
(74) Hu, X.; Brunschwig, B. S.; Peters, J. C. *J. Am. Chem. Soc.* **2007**, *129*, 8988−8998.
(75) Baffert, C.; Artero, V.; Fontecave, M. *Inorg. Chem.* **2007**, *46*, 1817−1824.
(76) Dempsey, J. L.; Brunschwig, B. S.; Winkler, J. R.; Gray, H. B. *Acc. Chem. Res.* **2009**, *42*, 1995−2004.
(77) Dempsey, J. L.; Winkler, J. R.; Gray, H. B. *J. Am. Chem. Soc.* **2010**, *132*, 16774−16776.
(78) Jacques, P.-A.; Artero, V.; Pécaut, J.; Fontecave, M. *Proc. Natl. Acad. Sci. U.S.A.* **2009**, *106*, 20627−20632.
(79) McCrory, C. C. L.; Uyeda, C.; Peters, J. C. *J. Am. Chem. Soc.* **2012**, *134*, 3164−3170.
(80) Solis, B. H.; Yu, Y.; Hammes-Schiffer, S. *Inorg. Chem.* **2013**, *52*, 6994−6999.
(81) Gjerde, H. B.; Espenson, J. H. *Organometallics* **1982**, *1*, 435−440.
(82) Bakac, A.; Espenson, J. H. *J. Am. Chem. Soc.* **1984**, *106*, 5197−5202.
(83) Pantani, O.; Anxolabéhère-Mallart, E.; Aukauloo, A.; Millet, P. *Electrochem. Commun.* **2007**, *9*, 54−58.
(84) Rose, M. J.; Winkler, J. R.; Gray, H. B. *Inorg. Chem.* **2012**, *51*, 1980−1982.
(85) Rose, M. J.; Gray, H. B.; Winkler, J. R. *J. Am. Chem. Soc.* **2012**, *134*, 8310−8313.
(86) Hratchian, H. P.; Schlegel, H. B. *J. Chem. Theory Comput.* **2005**, *1*, 61−69.
(87) Sonnenberg, J. L.; Wong, K. F.; Voth, G. A.; Schlegel, H. B. *J. Chem. Theory Comput.* **2009**, *5*, 949−961.
(88) Gao, J.; Truhlar, D. G. *Annu. Rev. Phys. Chem.* **2002**, *53*, 467−505.
(89) Truhlar, D. G.; Garrett, B. C. Variational Transition State Theory in the Treatment of Hydrogen Transfer Reactions. In *Hydrogen Transfer Reactions*; Hynes, J. T., Klinman, J. P., Limbach, H.-H., Schowen, R. L., Eds.; Wiley-VCH Verlag GmbH & Co. KGaA: Weinheim, Germany, 2007.
(90) Voth, G. A. Path-Integral Centroid Methods in Quantum Statistical Mechanics and Dynamics. In *Advances in Chemical Physics: New Methods in Computational Quantum Mechanics*; Prigogine, I., Rice, S. A., Eds.; John Wiley & Sons, Inc.: Hoboken, NJ, 2007; Vol. 93.
(91) Braun-Sand, S.; Olsson, M. H. M.; Mavri, J.; Warshel, A. Computer Simulations of Proton Transfer in Proteins and Solutions. In *Hydrogen-Transfer Reactions*; Hynes, J. T., Klinman, J. P., Limbach, H.-H., Schowen, R. L., Eds.; Wiley-VCH Verlag GmbH & Co. KGaA: Weinheim, Germany, 2007.
(92) Billeter, S. R.; Webb, S. P.; Iordanov, T.; Agarwal, P. K.; Hammes-Schiffer, S. *J. Chem. Phys.* **2001**, *114*, 6925−6936.
(93) Marcus, R. A. *Annu. Rev. Phys. Chem.* **1964**, *15*, 155−196.
(94) Marcus, R. A. *J. Phys. Chem.* **1968**, *72*, 891−899.
(95) Jakobsen, S.; Mikkelsen, K. V.; Pedersen, S. U. *J. Phys. Chem.* **1996**, *100*, 7411−7417.
(96) Marcus, R. A. *J. Chem. Phys.* **1965**, *43*, 679−701.
(97) Liu, Y.-P.; Newton, M. D. *J. Phys. Chem.* **1994**, *98*, 7162−7169.
(98) Grahame, D. C. *Chem. Rev.* **1947**, *41*, 441−501.
(99) Bard, A. J.; Faulkner, L. R. *Electrochemical Methods: Fundamentals and Applications*, 2nd ed.; John Wiley & Sons, Inc.: New York, 2001.
(100) Ghosh, S.; Horvath, S.; Soudackov, A. V.; Hammes-Schiffer, S. 2014, DOI: 10.1021/ct500051e.
(101) Sebastian, K. L. *J. Chem. Phys.* **1989**, *90*, 5056−5067.
(102) Boroda, Y. G.; Voth, G. A. *J. Electroanal. Chem.* **1998**, *450*, 95−107.
(103) Kuznetsov, A. M.; Schmickler, W. *Chem. Phys. Lett.* **2000**, *327*, 314−318.
(104) Hartnig, C.; Koper, M. T. M. *J. Am. Chem. Soc.* **2003**, *125*, 9840−9845.
(105) Dominguez-Ariza, D.; Hartnig, C.; Sousa, C.; Illas, F. *J. Chem. Phys.* **2004**, *121*, 1066−1073.
(106) Schmickler, W. *Electrochim. Acta* **1996**, *41*, 2329−2338.
(107) Gosavi, S.; Marcus, R. A. *J. Phys. Chem. B* **2000**, *104*, 2067−2072.
(108) Hewson, A. C.; Meyer, D. *J. Phys.: Condens. Matter* **2002**, *14*, 427−445.
(109) Lundin, U.; McKenzie, R. H. *Phys. Rev. B* **2002**, *66*, 075303.
(110) Yeganeh, S.; Ratner, M. A.; Mujica, V. *J. Chem. Phys.* **2007**, *126*, 161103.
(111) Soudackov, A.; Hammes-Schiffer, S. *J. Chem. Phys.* **2000**, *113*, 2385−2396.
(112) Soudackov, A.; Hatcher, E.; Hammes-Schiffer, S. *J. Chem. Phys.* **2005**, *122*, 014505.
(113) Venkataraman, C.; Soudackov, A. V.; Hammes-Schiffer, S. *J. Phys. Chem. C* **2008**, *112*, 12386−12397.
(114) Navrotskaya, I.; Hammes-Schiffer, S. *J. Chem. Phys.* **2009**, *131*, 024112.
(115) Auer, B.; Fernandez, L. E.; Hammes-Schiffer, S. *J. Am. Chem. Soc.* **2011**, *133*, 8282−8292.
(116) Horvath, S.; Fernandez, L. E.; Soudackov, A. V.; Hammes-Schiffer, S. *Proc. Natl. Acad. Sci. U.S.A.* **2012**, *109*, 15663−15668.
(117) Hammes-Schiffer, S.; Hatcher, E.; Ishikita, H.; Skone, J. H.; Soudackov, A. V. *Coord. Chem. Rev.* **2008**, *252*, 384−394.
(118) DuBois, M. R.; DuBois, D. L. *C. R. Chim.* **2008**, *11*, 805−817.
(119) DuBois, M. R.; DuBois, D. L. *Chem. Soc. Rev.* **2009**, *38*, 62−72.
(120) Le Goff, A.; Artero, V.; Jousselme, B.; Tran, P. D.; Guillet, N.; Métayé, R.; Fihri, A.; Palacin, S.; Fontecave, M. *Science* **2009**, *326*, 1384−1387.
(121) Yang, J. Y.; Bullock, R. M.; DuBois, M. R.; DuBois, D. L. *MRS Bull.* **2011**, *36*, 39−47.
(122) Tye, J. W.; Darensbourg, M. Y.; Hall, M. B. *J. Comput. Chem.* **2006**, *27*, 1454−1462.
(123) Gloaguen, F.; Rauchfuss, T. B. *Chem. Soc. Rev.* **2009**, *38*, 100−108.
(124) Tard, C.; Pickett, C. J. *Chem. Rev.* **2009**, *109*, 2245−2274.
(125) Capon, J.-F.; Gloaguen, F.; Pétillion, F. Y.; Schollhammer, P.; Talarmin, J. *Coord. Chem. Rev.* **2009**, *253*, 1476−1494.
(126) Yang, X.; Hall, M. B. *J. Am. Chem. Soc.* **2009**, *131*, 10901−10908.
(127) Liu, T.; Li, B.; Popescu, C. V.; Bilko, A.; Pérez, L. M.; Hall, M. B.; Darensbourg, M. Y. *Chem.—Eur. J.* **2010**, *16*, 3083−3089.
(128) Onuchic, J. N.; Beratan, D. N.; Winkler, J. R.; Gray, H. B. *Annu. Rev. Biophys. Biomol. Struct.* **1992**, *21*, 349−377.
(129) Peters, J. W. *Curr. Opin. Struct. Biol.* **1999**, *9*, 670−676.
(130) Frey, M. *ChemBioChem* **2002**, *3*, 153−160.
(131) Fontecilla-Camps, J. C.; Volbeda, A.; Cavazza, C.; Nicolet, Y. *Chem. Rev.* **2007**, *107*, 4273−4303.
(132) Carroll, M. E.; Barton, B. E.; Rauchfuss, T. B.; Carroll, P. J. *J. Am. Chem. Soc.* **2012**, *134*, 18843−18852.
(133) DuBois, D. L.; Bullock, R. M. *Eur. J. Inorg. Chem.* **2011**, 1017−1027.
(134) Kilgore, U. J.; Stewart, M. P.; Helm, M. L.; Dougherty, W. G.; Kassel, W. S.; DuBois, M. R.; DuBois, D. L.; Bullock, R. M. *Inorg. Chem.* **2011**, *50*, 10908−10918.
(135) Helm, M. L.; Stewart, M. P.; Bullock, R. M.; DuBois, M. R.; DuBois, D. L. *Science* **2011**, *333*, 863−866.
(136) Fraze, K.; Wilson, A. D.; Appel, A. M.; DuBois, M. R.; DuBois, D. L. *Organometallics* **2007**, *26*, 3918−3924.
(137) Chen, S.; Ho, M.-H.; Bullock, R. M.; DuBois, D. L.; Dupuis, M.; Rousseau, R.; Raugei, S. *ACS Catal.* **2014**, *4*, 229−242.
(138) Appel, A. M.; Pool, D. H.; O'Hagan, M.; Shaw, W. J.; Yang, J. Y.; DuBois, M. R.; DuBois, D. L.; Bullock, R. M. *ACS Catal.* **2011**, *1*, 777−785.
(139) O'Hagen, M.; Shaw, W. J.; Raugei, S.; Chen, S.; Yang, J. Y.; Kilgore, U. J.; DuBois, D. L.; Bullock, R. M. *J. Am. Chem. Soc.* **2011**, *133*, 14301−14312.
(140) Fernandez, L. E.; Horvath, S.; Hammes-Schiffer, S. *J. Phys. Chem. Lett.* **2013**, *4*, 542−546.

NOTE ADDED AFTER ASAP PUBLICATION

Due to a production error, this paper was published on the Web on April 14, 2014, with minor text errors. The corrected version was reposted on April 17, 2014.

dx.doi.org/10.1021/ic5002896 | *Inorg. Chem.* 2014, 53, 6427−6443